JOURNAL OF GEOPHYSICAL RESEARCH, VOL. 111, D17103, doi:10.1029/2005JD006700, 2006

Response of water vapor and clouds to El Niño warming in three National Center for Atmospheric Research atmospheric models

Tao Zhang[1] and De-Zheng Sun[1]

Received 22 September 2005; revised 12 April 2006; accepted 12 May 2006; published 7 September 2006.

[1] The response of water vapor and clouds to El Niño warming over the tropical Pacific in the most recent three versions of the National Center for Atmospheric Research (NCAR) Community Atmosphere Model (CAM2, T42 CAM3, and T85 CAM3) is quantified and compared to observations. It is found that all three models have a stronger response in the greenhouse effect of water vapor than that indicated in Earth Radiation Budget Experiment (ERBE) observations. The overestimate is most severe in the T85 CAM3 (up to 36%). Compared with National Centers for Environmental Prediction (NCEP) reanalysis, all three models have an excessive response of atmospheric moisture content in the upper troposphere, suggesting a cause for the excessive response in the greenhouse effect of water vapor. The response in the greenhouse effect of clouds (the longwave forcing of clouds) in two of the models (CAM2 and T42 CAM3) is significantly weaker than that indicated in ERBE observations, but it is comparable to the observed in the T85 CAM3. The improvement in the T85 CAM3 in simulating the response in the greenhouse effect is helped by a stronger response in the middle level clouds in the model (compared to CAM2 and T42 CAM3). In contrast to the strong negative response in the shortwave forcing seen in the ERBE observations, the response of the shortwave forcing of clouds in the CAM2 and the T42 CAM3 is weak and even has a sign opposite to observations when it is averaged over the entire region of surface warming. The simulation of the response of the shortwave forcing in the T85 CAM3 is considerably improved, though the negative response over the equatorial Pacific is still not strong enough compared to ERBE observations. The stronger negative response in the shortwave forcing in the T85 CAM3 is apparently linked to a stronger response in the middle level cloud cover. All three models fail to simulate the observed pattern of the response in the low cloud cover over the central and eastern Pacific, resulting in deficiency in the response of the shortwave cloud forcing in that region. The deficiency in the low cloud cover response suggests that the low cloud cover scheme has room for improvement.

Citation: Zhang, T., and D.-Z. Sun (2006), Response of water vapor and clouds to El Niño warming in three National Center for Atmospheric Research atmospheric models, *J. Geophys. Res.*, *111*, D17103, doi:10.1029/2005JD006700.

1. Introduction

[2] Water vapor and clouds play a vital role in the radiation and heat budgets of the Earth-Atmosphere system. They are the major contributors to the greenhouse effect of Earth's atmosphere [*Kiehl and Trenberth*, 1997]. Clouds are also a major contributor to Earth's albedo [*Ramanathan and Collins*, 1991]. The stability and sensitivity of the climate system depend critically on the feedbacks from the water vapor and clouds. To predict the response of the climate system to anthropogenic forcing, climate models have to simulate correctly the feedbacks of water vapor and clouds. It is not clear, however, that these feedbacks are simulated correctly in the climate models [*Cess et al.*, 1990, 1996; *Stocker et al.*, 2001; *Sun et al.*, 2001].

[3] By examining the response of water vapor and clouds to ENSO forcing, *Sun et al.* [2003] noted that the feedback from the greenhouse effect of water vapor in the NCAR CCM3 [*Kiehl et al.*, 1998a] is overestimated relative to observations; the simulated feedback from cloud longwave forcing and solar forcing is also overestimated and underestimated separately in the model. These feedback biases contribute to the cold tongue SST bias in the coupled NCAR Climate System Model (CSM) [*Boville and Gent*, 1998] as they cause the regulating effect from the model atmosphere over the underlying SST to be much weaker than in reality.

[4] The purpose of this study is to extend the work by *Sun et al.* [2003] by looking at the water vapor and clouds response to ENSO forcing in more detail. Here we analyze three versions of NCAR climate model (CAM2 and CAM3

[1]Climate Diagnostics Center, Physical Science Division, Earth System Research Laboratory, NOAA-CIRES, Boulder, Colorado, USA.

at T42 and at T85 resolutions). We quantify the response of water vapor and clouds to El Niño warming over the tropical Pacific and diagnose the causes for the model deficiencies. In particular, the present work attempts to identify the effect of improved physical parameterizations on the response of water vapor and clouds to El Niño warming by comparing the results from CAM2 [*Collins et al.*, 2003] with those from CAM3 [*Collins et al.*, 2004, 2006a]. We also attempt to identify the effect of changes in horizontal resolution on the response of water vapor and clouds to El Niño warming by comparing the results from CAM3 at T85 resolution with those from the standard version of CAM3.

[5] On the basis of the satellite observations from the Earth Radiation Budget Experiment (ERBE) [*Barkstrom*, 1984], *Ramanathan and Collins* [1991] first observed that during El Niño year the greenhouse effect of water vapor increases in response to the positive SST anomaly. They also noted that more cirrus clouds are produced that reflect more solar radiation back to space. They proposed that this negative feedback from cloud albedo acts as a thermostat that regulates the maximum SST. Using ERBE data, *Chou* [1994] also performed an analysis of the changes in the radiation budgets for the tropical Pacific in response to 1987 El Niño. By averaging over the tropical Pacific region (30°S–30°N, 100°E–100°W), Chou found a negative water vapor feedback. He found that the observed clear-sky greenhouse effect is decreased by 1.3 W m^{-2} in going from the colder month of April 1985 to the warmer month of April 1987. He also noticed that the change in the net cloud forcing is small between April 1985 and April 1987 in that region. *Soden* [1997] repeated the calculations by *Chou* [1994] and confirmed a decrease in the tropical Pacific mean water vapor greenhouse effect between these two months. However, he observed a distinct increase in the tropical mean greenhouse trapping when the entire time series over the ERBE period is considered. Utilizing radiation data from ERBE and circulation data from NCEP reanalysis [*Kalnay et al.*, 1996] and assimilated ocean data [*Ji et al.*, 1995], *Sun and Trenberth* [1998] showed that the ocean warming during the 1986–1987 El Niño is not only accompanied by significant increases in the cloud reflection of the solar radiation, but also by marked increases in the poleward transport of energy in the atmosphere and ocean.

[6] The above studies have provided us a valuable observational background for evaluating the response of water vapor and clouds to El Niño warming in climate models. Here we focus our efforts on the NCAR models. Linked to the Community Climate System Model (CCSM) project [*Collins et al.*, 2006b], the NCAR Community Atmosphere Model (CAM) has been improved rapidly [*Collins et al.*, 2006a]. These improvements, the changes in the response of water vapor and clouds to El Niño warming in particular, have not been fully documented and examined. The hydrological aspects of the NCAR CCM3 were examined by *Hack et al.* [1998]. An updated study in the T85 CAM3 is presented by *Hack et al.* [2006a]. These studies focus on the seasonal and annual mean quantities. *Sun et al.* [2006] looked at the response of water vapor and clouds to El Niño warming from nine general circulation models (GCMs) including several NCAR models. However, they are more concerned with the net atmospheric feedback than with the individual feedbacks of water vapor and clouds, and only examine the greenhouse effect of water vapor and the radiative forcing of clouds and how well NCAR model in simulating the net atmospheric feedback relative to other models. We attempt here to provide a more detailed analysis including the three-dimensional field of water vapor and clouds.

[7] The paper is organized as follows: We describe the methodology and observations in section 2. A brief description of the models is also presented there. In section 3, we first compare the models' climatology with observations, and investigate the changes in greenhouse effect of water vapor and cloud radiative forcing in an El Niño episode. We then proceed to quantify the response of various fluxes using their interannual variability. We critically examine the spatial patterns of the observed and simulated responses and explore the possible cause of the discrepancies between models and observations. The conclusions and discussions are given in section 4.

2. Methodology, Data, and Model

[8] The greenhouse effect of water vapor at the top of the atmosphere (TOA) can be quantified as [*Raval and Ramanathan*, 1989]

$$G_a = \sigma T_s^4 - LW_{clear} \tag{1}$$

Following *Charlock and Ramanathan* [1985], the longwave and shortwave cloud forcing at the TOA are defined as

$$C_l = LW_{clear} - LW \tag{2}$$

$$Cs = SW - SW_{clear} \tag{3}$$

Where σ is the Stefan-Boltzmann constant. Ts is the SST. We assume the surface emissivity to be unity (we consider only ocean regions in this study). LW_{clear} and LW are the clear-sky and all-sky TOA longwave flux, defined as positive upward. SW_{clear} and SW are the clear-sky and all-sky TOA net downward solar radiation flux separately.

[9] Using the observed interannual anomaly of SST averaged over the region of El Niño warming (160°–290°E, 5°S–5°N) as an index [*Sun et al.*, 2003], we can quantify the responses by linearly regressing the variations of above fluxes against this SST index, following the same way as by *Sun et al.* [2003].

[10] The observed radiation fluxes at the TOA are obtained from ERBE [*Barkstrom*, 1984]. Observations of cloud cover are obtained from the International Satellite Cloud Climate Project (ISCCP) data [*Rossow et al.*, 1996; *Rossow and Schiffer*, 1999]. Note that in obtaining the middle and low cloud level, ISCCP cloud cover has been adjusted for cloud layering assuming a random cloud overlap. The detailed discussion of ISCCP cloud overlap is given by *Sun et al.* [2003]. The specific humidity data from the National Centers for Environmental Prediction–National Center for Atmospheric Research (NCEP-NCAR) reanalysis [*Kalnay et al.*, 1996] are also used in the present study. Observations of precipitation are obtained from the CPC Merged Analysis of Precipitation (CMAP) [*Xie and Arkin*, 1997] data archived in Climate Diagnostics branch of the Physical Sciences Division (PSD) of the Earth System

Research Laboratory (ESRL), NOAA (see http://www.cdc.noaa.gov/cdc/data.cmap.html). We use the standard monthly data in this paper that just include 5 kinds of satellite estimates (GOES precipitation index (GPI), OLR-based precipitation index (OPI), the special sensor microwave imager (SSM/I) scattering, SSM/I emission and microwave sounding unit (MSU)). The model integrations from three models are performed using observed SSTs as prescribed by the Atmospheric Model Intercomparison Project [*Gates*, 1992].

[11] The NCAR Community Atmosphere Model (CAM2) is a global atmospheric general circulation model developed from the NCAR CCM3 [*Kiehl et al.*, 1998a]. The CAM2 remains the same horizontal T42 (~2.875°) resolution as the CCM3, but it has 26 levels in the vertical as compared to the 18 levels in CCM3. The additional 8 levels are added near the tropopause. The physics in the CAM2 has several important changes. A prognostic formulation for cloud water [*Rasch and Kristjansson*, 1998] is included in the CAM2 in place of the diagnostic prescription used in CCM3. The total cloud water is predicted based on the model grid box temperature and this condensate combines the liquid and ice phases. This scheme can deal with a much broader variability of cloud condensate than the previous scheme, which prescribed the vertical distribution of condensate based upon the column-integrated water vapor.

[12] The cloud fraction for the CAM2 is based on a diagnostic Slingo-type scheme [*Slingo*, 1987] similar to the CCM3. Cloud fraction depends on relative humidity, vertical velocity, static stability, and convective mass fluxes. Clouds can exist at all tropospheric levels above the surface. Three types of cloud are diagnosed including low-level marine stratus, convective cloud, and layered cloud. The low-level marine stratus is derived by *Klein and Hartmann* [1993] using an empirical seasonal relationship between marine stratus cloud fraction and the potential temperature difference between 700 mbar and the surface. The convective cloud fraction is made proportional to the convective detrainment rate above 500 hpa following *Rasch and Kristjansson* [1998]. The layered clouds are formed when the relative humidity exceeds a threshold value which varies according to pressure, atmospheric stability and large-scale vertical velocity [*Collins et al.*, 2003].

[13] A new generalized geometrical cloud overlap scheme [*Collins*, 2001] is incorporated in CAM2 to allow a greater variety of cloud overlap assumptions. It is assumed that adjacent clouds layers are maximally overlapped and groups of clouds separated by cloud-free layers are randomly overlapped. The improvements also involve more accurate treatment of the absorption and emission of infrared radiation by water vapor [*Collins et al.*, 2002]. The CKD continuum version 2.1 by *Clough et al.* [1989] is used to treat the longwave properties of water vapor. Although it improves the simulation of longwave fluxes and cooling rates, this updated scheme leads to an enhanced longwave cooling in the upper troposphere and thus affects the convective activity whose change contributes to a significant drying of tropical atmosphere. In order to reduce this drying deficiency, the CAM2 includes the evaporation of convective precipitation back to the atmosphere which is proportional to the relative humidity in a given model layer [*Kiehl and Gent*, 2004]. The CAM2 retains the *Zhang and McFarlane* [1995] parameterization for deep moist convection, while shallow dry convection is treated using the Hack scheme [*Hack*, 1994]. The Zhang and McFarlane scheme assumes that an ensemble of convective-scale updrafts may occur whenever the lower atmosphere is conditionally unstable. Moist convection occurs only when there is convective available potential energy (CAPE) for which parcel ascent from the subcloud layer acts to destroy the CAPE at an exponential rate using a specified adjustment timescale (=2 h) [*Collins et al.*, 2003].

[14] With the same 26 levels in the vertical as the CAM2, three standard configurations of the CAM3 are distributed including horizontal spectral truncations of T31 (~3.75°), T42 (~2.875°), and T85 (~1.4°). Presented in this study are the results from the T42 CAM3 and the T85 CAM3. The detailed description of the CAM3 is given by *Collins et al.* [2004, 2006a] and *Hack et al.* [2006b]. The main differences between CAM3 and CAM2 pertinent to this study are briefly described below. The *Rasch and Kristjansson* [1998] prognostic cloud water scheme in CAM2 predicts a total cloud condensate variable that is the sum of the liquid and ice phase condensate, but the CAM3 includes separate prognostic treatments of liquid and ice condensate based on the consideration that their microphysical and radiative properties are very different [*Boville et al.*, 2006]. The advection and sedimentation of cloud condensate are also included in the equations governing cloud condensate in CAM3, but they are ignored in CAM2. The modifications also include the detrainment of cloud condensate. Condensed water detrained from shallow and deep convection can either form precipitation or additional stratiform cloud water. In CAM2, all of the detrained condensate from the shallow convection and part of that from the deep convection evaporate into the environment rather detraining into clouds. In CAM3, all of the condensate is detrained into the clouds. The major change in the cloud fraction parameterization lies in the parameterization of convective cloud fraction, which is related to updraft mass flux in the deep and shallow cumulus schemes according to a functional form suggested by *Xu and Krueger* [1991] in the CAM3. The changes to the moist processes between CAM2 and CAM3 are fully documented by *Boville et al.* [2006]. Modifications to longwave interaction with water vapor are also included in the CAM3. The shortwave absorption by water vapor has been updated in the CAM3. In the original shortwave parameterization for CAM2 [*Briegleb*, 1992], the absorption by water vapor is derived from the calculations by *Ramaswamy and Freidenreich* [1991]. The original parameterization in the CAM2 did not include the effects of the water vapor continuum in the visible and near-infrared. In the CAM3, it incorporates the CKD model version 2.4 [*Clough et al.*, 1989] prescription for the continuum [*Collins et al.*, 2004]. The CAM3 still retains the *Zhang and McFarlane* [1995] parameterization for deep moist convection and the Hack scheme [*Hack*, 1994] for the shallow dry convection.

3. Results

3.1. Model Climatology Validation

[15] Before we focus on the analysis of response to El Niño warming, we first take a look at the annual mean

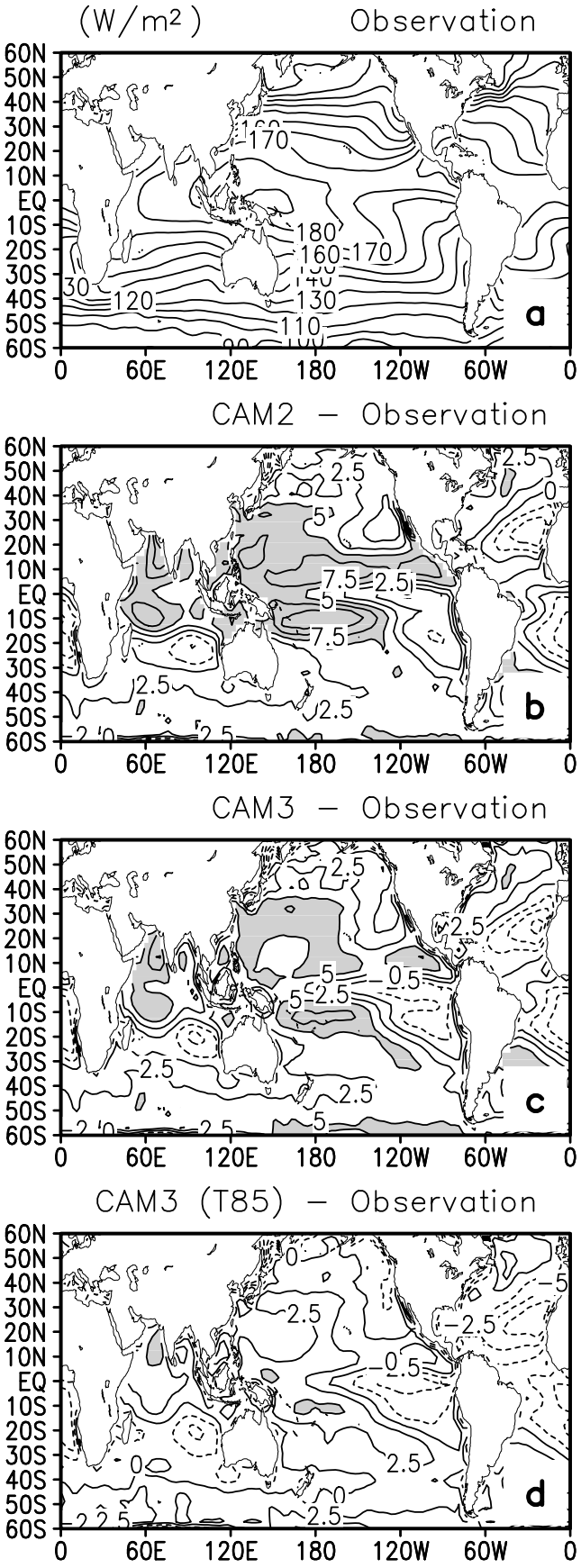

Figure 1. (a) Geographical distributions of annual mean greenhouse effect of water vapor (Ga) from ERBE observations, (b) the difference between CAM2 and observations, (c) the difference between T42 CAM3 and observations, and (d) the difference between T85 CAM3 and observations over the ERBE period.

climatology of water vapor and clouds in the models. Globally, the annual mean greenhouse effect of water vapor (Ga) for the TOA in the NCAR CAM2 (142.6 W m^{-2}) is in good agreement with the ERBE observed (142.4 W m^{-2}), the two NCAR CAM3 models also have very close values (139.8 W m^{-2} in the T42 CAM3 and 138.2 W m^{-2} in the T85 CAM3) to the observed but with a slight underestimation of 2.6 W m^{-2} and 4.2 W m^{-2}, respectively. As suggested by *Raval and Ramanathan* [1989], the error (systematic plus random) in the monthly and regional mean values of Ga is expected to be 5 to 10 W m^{-2} because ERBE TOA longwave fluxes have an estimated systematic error of about 5 W m^{-2} for monthly averaged values due to cloud contamination [*Barkstrom*, 1984; *Ramanathan et al.*, 1989].

[16] Figure 1 shows the geographical distributions of the annual mean climatology of Ga. The observed Ga exhibits a maximum over the relatively warm western Pacific and a minimum over the cold eastern Pacific together with a decrease from the equator to pole (Figure 1a). This is because Ga is strongly correlated with surface temperature [*Raval and Ramanathan*, 1989]. The three models can capture the observed pattern very well but overestimate the magnitude of greenhouse effect by about 5–10 W m^{-2} in the CAM2 and the T42 CAM3 (Figures 1b and 1c) and about less than 5 W m^{-2} in the T85 CAM3 (Figure 1d) over the western Pacific and Indian Ocean. This contributes to the errors that the tropical mean (30°S–30°N) of Ga in these two models (170.9 W m^{-2} in the CAM2 and 169.0 W m^{-2} in the T42 CAM3) is 2–3 W m^{-2} higher than that in observations (167.4 W m^{-2}). The match of the tropical mean of Ga in the T85 CAM3 (167.3 W m^{-2}) with the observed value is due to the perfect cancellation between the reduced positive biases over the western Pacific and Indian Ocean and the increased negative biases over the Pacific cold tongue and the Atlantic.

[17] The associated atmospheric moisture amounts (specific humidity) in the upper troposphere (500 hPa) and the low troposphere (850 hPa) are shown in Figure 2. Compared to the NCEP reanalysis, the three models apparently overestimate the atmospheric moisture over the western Pacific and Indian Ocean, and the overestimate is especially obvious in two CAM3 models in the upper troposphere (Figures 2c and 2d). The contributions from the biases in the low troposphere appear to be relatively weaker (Figures 2f–2h). The overestimate of the moisture in the upper troposphere may contribute significantly to the overestimation of Ga in the models. However, it should be noted that measured by the column-integrated atmospheric water vapor amount known as precipitable water, the NCEP reanalysis data are somewhat lower than the satellite data–SSM/I data set from remote sensing systems (RSS) [see *Wentz*, 1997] in most of tropical oceans [*Trenberth et al.*, 2005]. It is well-known that global observational data

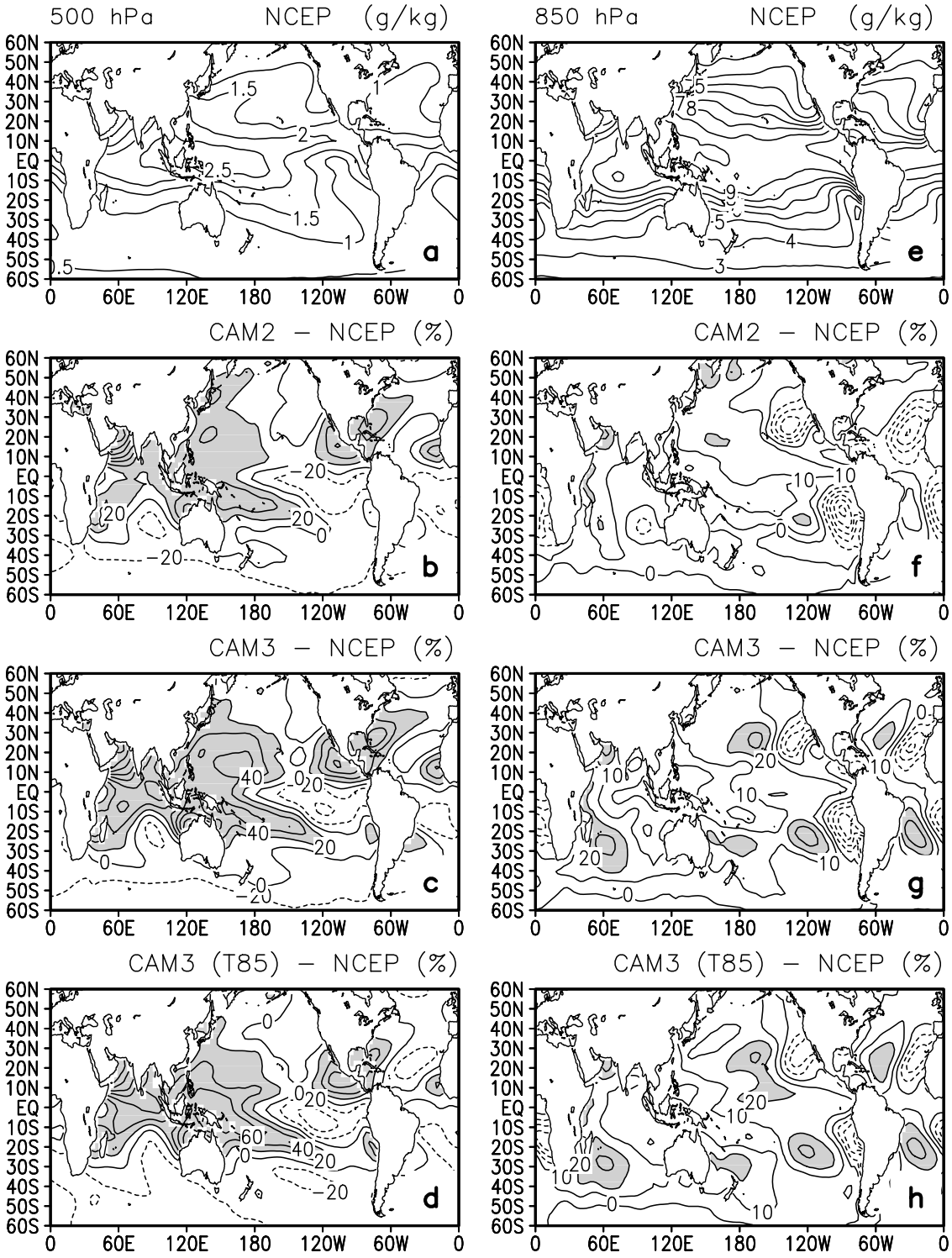

Figure 2. (a) Geographical distributions of annual mean specific humidity in the upper troposphere (500 hPa) from the NCEP-NCAR reanalysis and the percentage differences between (b) CAM2, (c) T42 CAM3, (d) T85 CAM3 and NCEP data over the ERBE period. The percentage differences are obtained from the differences between models and NCEP data divided by the values of NCEP data. (e–h) Corresponding annual mean specific humidity in the low troposphere (850 hPa), respectively.

on the vertical distribution of atmospheric water vapor are difficult to find, and the reanalysis products provide the best available estimates [*Hack et al.*, 2006a]. We have obtained the similar results by using the European Centre for Medium-Range Weather Forecasts (ECMWF) reanalyses ERA-40 [*Uppala et al.*, 2005]. The too large Ga in the models over the western Pacific and Indian Ocean could be in part due to the fact that the satellite data are biased

toward excessively dry conditions [*Hartmann et al.*, 1992; *Collins and Inamdar*, 1995] and may underestimate the greenhouse effect of water vapor.

[18] The global mean cloud longwave radiative forcing (Cl) for the TOA in the models (30.2 W m^{-2} in the CAM2, 30.7 W m^{-2} in the T42 CAM3, and 32.1 W m^{-2} in the T85 CAM3) is very close to the observed value of 31.6 W m^{-2}, and the corresponding cloud solar forcing (Cs) for the TOA in the models (-55.7 W m^{-2} in the CAM2, -59.0 W m^{-2} in the T42 CAM3, and -59.7 W m^{-2} in the T85 CAM3) is also comparable to the observed (-60.1 W m^{-2}) except for a small underestimation in the CAM2. The spatial pattern of annual mean Cl and Cs is shown in Figure 3. It can be seen that the observed greenhouse effect of clouds also shows a maximum over the deep convection region of western Pacific and a minimum over the cold oceanic upwelling region (Figure 3a), which resembles the pattern of observed greenhouse effect of water vapor (Figure 1a) but with reduced magnitude. The simulated greenhouse effect of clouds from the CAM2 and the T42 CAM3 is underestimated over the western equatorial Pacific but overestimated over the subtropical Pacific and the eastern equatorial Pacific (Figures 3b and 3c). The Cl in the T85 CAM3 is about more than 10 W m^{-2} overestimated in the western Pacific, Indian Ocean, and the eastern equatorial Pacific (Figure 3d). This overestimation of Cl over the eastern equatorial Pacific is also present in the CCM3 simulation [*Kiehl et al.*, 1998b]. However, due to the cancellation of positive and negative biases, the tropical mean Cl from the CAM2 and the T42 CAM3 (30.7 W m^{-2} in the CAM2 and 31.5 W m^{-2} in the T42 CAM3) is still in line with ERBE (32.2 W m^{-2}). The slight overestimation (3.7 W m^{-2}) of tropical mean Cl from the T85 CAM3 is expected, since the dominant positive biases overwhelm the negative biases over the Pacific cold tongue and the Atlantic. The observed cloud solar forcing has a negative cooling effect on the climate system (Figure 3e) so that it has a near cancellation of the cloud longwave forcing in tropical regions [*Kiehl*, 1994]. The observed pattern of cooling effect of Cs is also reasonably captured in the models. Except for the underestimation over the western equatorial Pacific and equatorial Indian Ocean (positive biases) in the CAM2 and the T42 CAM3, the magnitude of cooling effect of Cs is overestimated (shaded negative biases) over most of ocean regions including the equatorial eastern Pacific and subtropical regions (Figures 3f–3h), which may contribute to the larger tropical mean values in the models (-54.9 W m^{-2} in the CAM2, -57.3 W m^{-2} in the T42 CAM3, and -61.5 W m^{-2} in the T85 CAM3) compared to ERBE (-52.0 W m^{-2}). The comparison of Cl and Cs also shows that the three models exhibit a bias with opposite sign in most regions, suggesting a same trend that the simulated Cl and Cs are biased toward. Specifically, the overestimated heating effect of Cl is located in the region where there is an overestimated cooling effect of Cs, and the underestimated heating effect of Cl is located in the region where there is an underestimated cooling effect of Cs.

[19] The observed and simulated time mean upper cloud cover are shown in Figure 4. It can be seen that the observed ISCCP high cloud occurs preferentially in the tropical convection region [*Hartmann et al.*, 1992] and the maximum locates in the western deep convection region (Figure 4a), but the CAM2 and the T42 CAM3 apparently overestimate the high cloud amount too much (Figures 4b and 4c). The overestimation of high cloud amount in these two models is not expected since the simulated Cl is underestimated especially in the tropical deep convection region (Figures 3b and 3c), which means that cloud amount is not the unique factor affecting the cloud forcing, the effect of cloud optical depth maybe plays a role [*Kiehl*, 1994]. However, the overestimation of high cloud amount in the T85 CAM3 (Figure 4d) is consistent with the stronger Cl in the tropical deep convection region (Figure 3d). The observed middle cloud cover resembles the high cloud cover very much both in pattern and magnitude (Figure 5a), the CAM2 is found to somewhat underestimate the middle cloud amount in the tropics (Figure 5b) but two CAM3 models have a better simulation (Figures 5c and 5d). The observed low cloud cover exhibits an enhanced magnitude than high and middle cloud cover and features a minimum in the eastern Pacific (Figure 5e), consistent with the low Cs over that region (Figure 3e). Considering that the maximum of middle cloud cover is in agreement with that of Cs over the western Pacific (Figures 5a and 3e), it is inferred that the Cs over the western Pacific may be dominated by the middle cloud cover while the Cs over the eastern Pacific may be dominated by the low cloud cover. The models fail to reproduce the minimum center of the low cloud cover in the eastern Pacific (indicated by the shaded positive biases in Figures 5f–5h), leading to an excessive cooling effect of Cs over that region (Figures 3f–3h).

[20] In general, the three NCAR models are capable of reproducing the global mean and tropical mean values of observed greenhouse effect of water vapor and cloud radiative forcing with reasonable accuracy. However, it appears that in many cases the correct mean values result from the cancellation of significant local errors. The Ga is overestimated over the western Pacific and Indian Ocean especially in the CAM2 and the T42 CAM3. The cooling effect of Cs is overestimated in most regions, except the western equatorial Pacific and equatorial Indian Ocean. The sign of Cl bias is opposite to that of Cs bias over most of oceans. The simulated high cloud amount is excessively high in the tropical convection region.

3.2. Difference Between April 1987 and April 1985

[21] We now contrast the differences between the two phases of ENSO in water vapor and clouds. Figure 6 shows the change in Ga between the warm (El Niño) month of April 1987 and the cold (La Niña) month of April 1985 [*Chou*, 1994; *Soden*, 1997] from observations and the differences between models and observations. The observed change of 10$\sim$15 W m^{-2} in Ga displays an enhanced effect over the central and eastern equatorial Pacific. The three models capture the positive response of Ga over the warming region, while the magnitudes of the change in Ga from the models are overestimated by 5$\sim$10 W m^{-2} especially in two CAM3 models. Over the subtropics, both the CAM2 and T42 CAM3 underestimate the decrease in Ga by over 10 W m^{-2} (positive biases). These biases are somewhat reduced in the T85 CAM3. Apparently, the overestimate of the change in the upper tropospheric moisture from three models contributes to the overestimate of the change in Ga over the equatorial Pacific. Figure 7 shows the differences

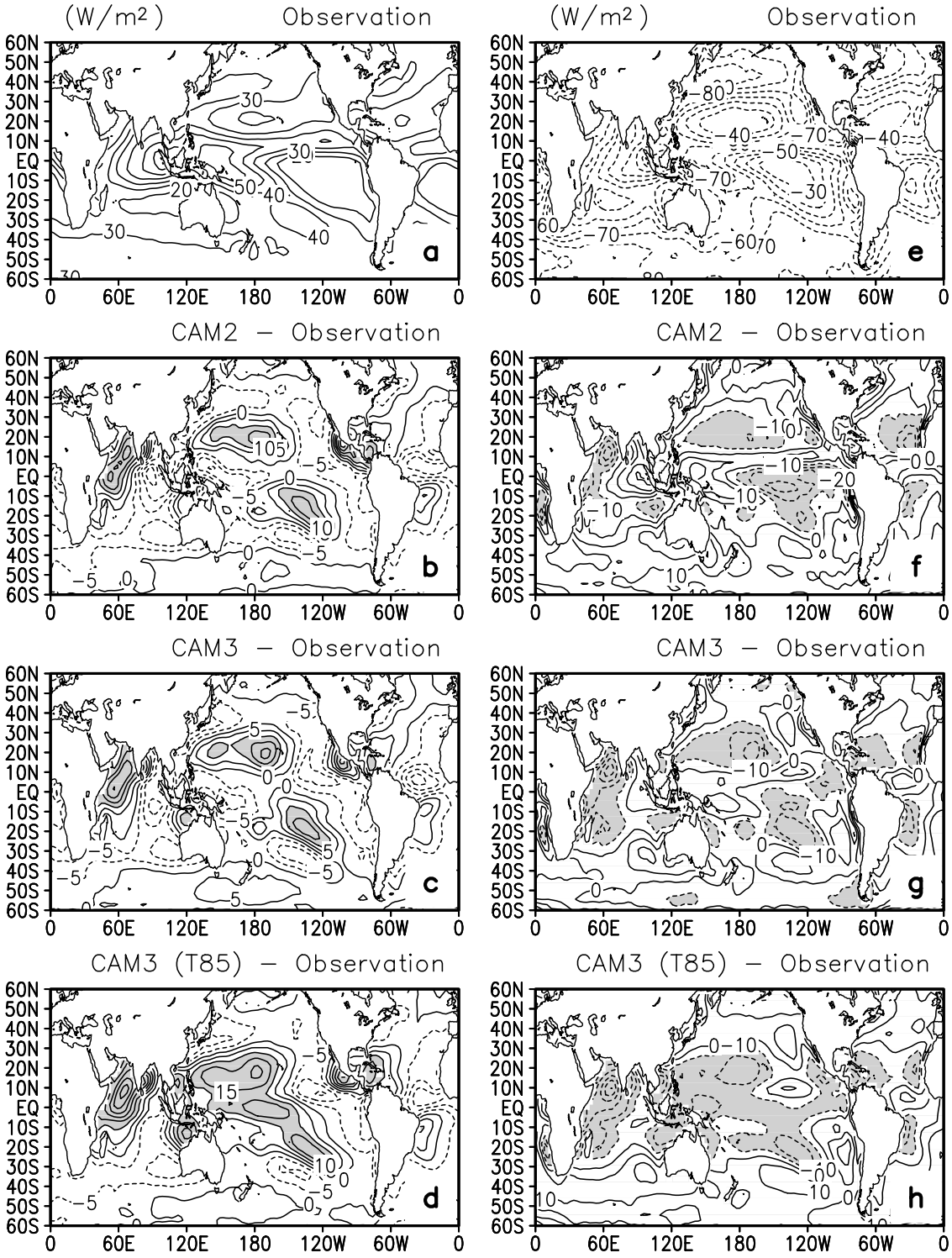

Figure 3. (a) Geographical distributions of annual mean greenhouse effect of clouds (Cl) from ERBE observations, (b) the difference between CAM2 and observations, (c) the difference between T42 CAM3 and observations, and (d) the difference between T85 CAM3 and observations over the ERBE period. (e–h) Corresponding annual mean cloud solar forcing (Cs).

(April 1987 minus April 1985) in atmospheric moisture (specific humidity) in the upper troposphere (500 hPa) and in precipitation. The stronger responses of atmospheric moisture in two CAM3 models over the equatorial Pacific (Figures 7c and 7d) are consistent with their relatively larger biases of Ga in that region (Figures 6c and 6d). The underestimate of the subtropical drying is more obvious in the CAM2 and T42 CAM3 (positive biases), which may

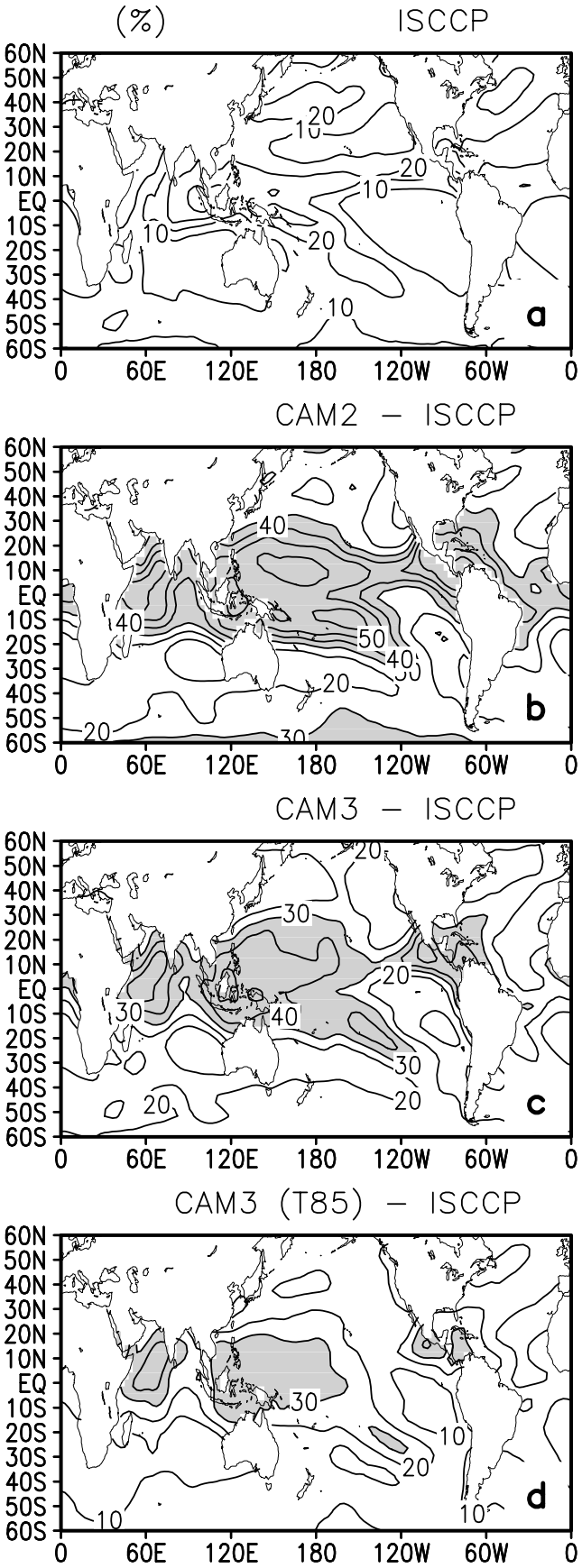

Figure 4. (a) Geographical distributions of annual mean high cloud amount from ISCCP observations, (b) the difference between CAM2 and observations, (c) the difference between T42 CAM3 and observations, and (d) the difference between T85 CAM3 and observations over the ERBE period.

contribute to the larger positive biases of changes in Ga in these two models over the subtropics. Interestingly, the response of precipitation in the models is weaker than the observed (Figures 7f–7h), suggesting a weaker convection intensity in the models. Thus the excessive response of atmospheric moisture in the models could be linked to the deficiency of the too frequent deep convection occurrence [*Xie et al.*, 2004; *Dai and Trenberth*, 2004].

[22] The differences in Ga between models and observations in April 1987 and in April 1985 are shown separately in Figures 8a–8d and 8e–8h. It shows that the models overestimate Ga by about 5∼10 W m^{-2} over the equatorial Pacific in the warm condition (Figures 8b–8d), while the differences between models and observations in the cold condition (Figures 8f–8h) are found to be small (less than 5 W m^{-2}). This suggests that the overestimation of the change in Ga from the NCAR models mainly comes from the positive bias in the warm El Niño condition. Consistent with the bias in Ga (Figure 8), the atmospheric moisture in the upper troposphere (500 hPa) is overestimated over the central and western Pacific during the warm phase in the models (Figures 9b–9d). Figure 9 also reveals that the models overestimate the atmospheric moisture in the wet region and underestimate it in the dry region. This deficiency is also present in the climatology (Figures 2b–2d). The errors in precipitation are more pronounced in the warm phase than in the cold phase (Figure 10).

[23] The observed and simulated changes in Cl from April 1985 to April 1987 are shown in Figure 11. Observations show a broad positive change over the equatorial Pacific, which is due to the more cloudiness in April 1987 causing a reduction in the OLR and an increase of Cl [*Chou*, 1994]. The observed pattern of the change in Cl (Figure 11a) is very similar to that of Ga (Figure 6a) but the magnitude is almost three times stronger. The observed positive change in Cl is simulated in the CAM2 and the T42 CAM3 over the equatorial Pacific, but the modeled magnitude is only half of the observed (Figures 11b and 11c). However, in the T85 CAM3 the magnitude of the change in Cl is greatly improved and the observed maximum over the central Pacific is well captured (Figure 11d). This model has a deficiency in the eastern Pacific where the modeled maximum is somewhat weakened and shifts eastward. The changes from April 1985 to April 1987 in the upper cloud cover are shown in Figure 12. The results show that the changes in high cloud cover are overestimated over the eastern equatorial Pacific especially in the CAM2 and the T42 CAM3. Therefore the underestimate of changes in Cl over the region of El Niño warming in these two models suggests possible biases in the cloud optical properties. The errors in changes of high cloud cover are somewhat reduced over the entire tropical Pacific in the T85 CAM3. It is found that the models overestimate the high cloud amount in both the warm and cold phase, and this overestimation is more

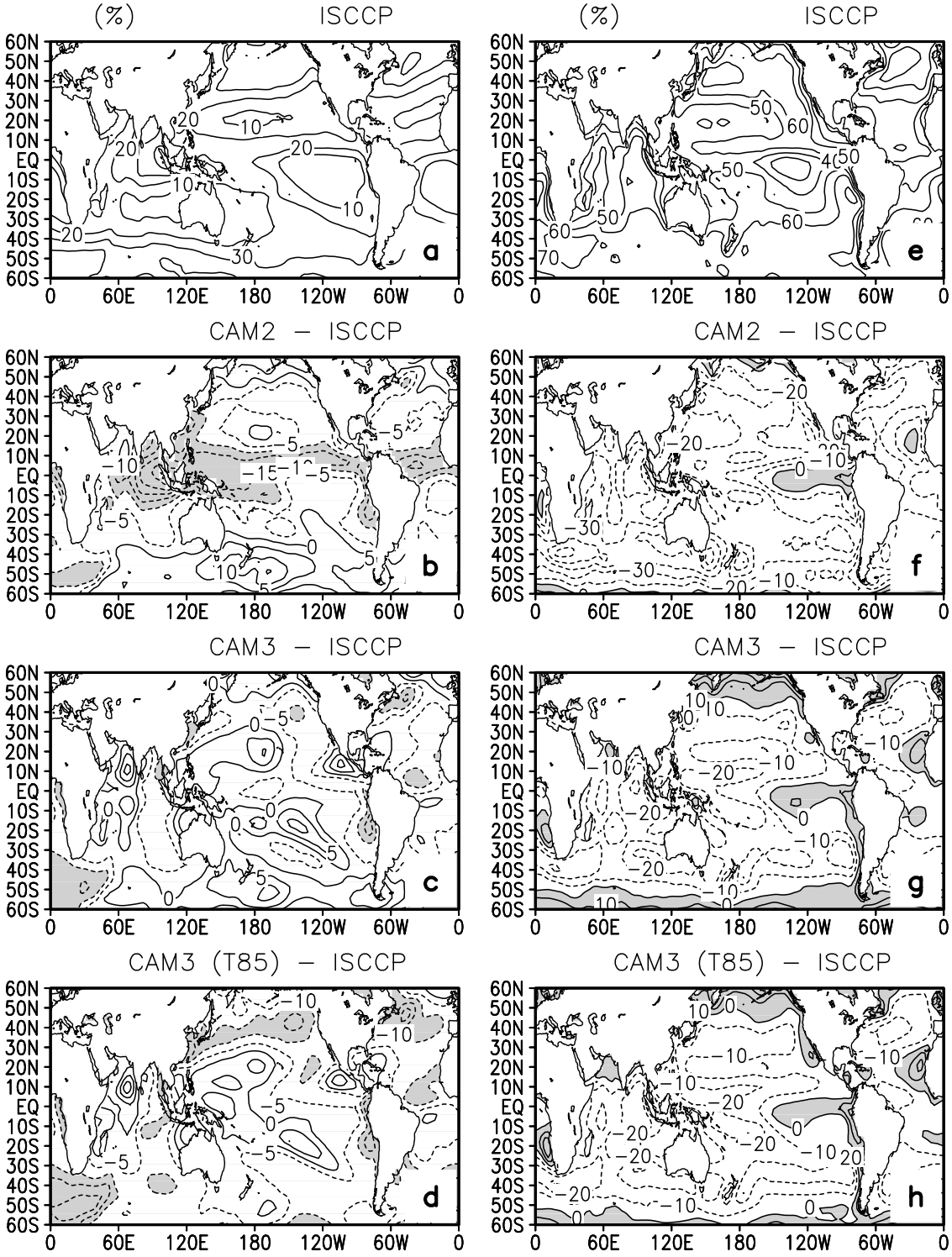

Figure 5. (a) Geographical distributions of annual mean middle cloud amount from ISCCP observations, (b) the difference between CAM2 and observations, (c) the difference between T42 CAM3 and observations, and (d) the difference between T85 CAM3 and observations over the ERBE period. (e–h) Corresponding annual mean low cloud amount.

pronounced in the CAM2 (Figure 13). The observations and the differences in Cl between models and observations for April 1987 and for April 1985 are shown in Figure 14. The underestimate of the change in Cl from the models is also found to originate from the simulation in the warm El Niño condition (Figures 14b–14d), and the differences between models and observations in the cold La Niña condition are small over the equatorial Pacific (Figures 14f–14h). Note

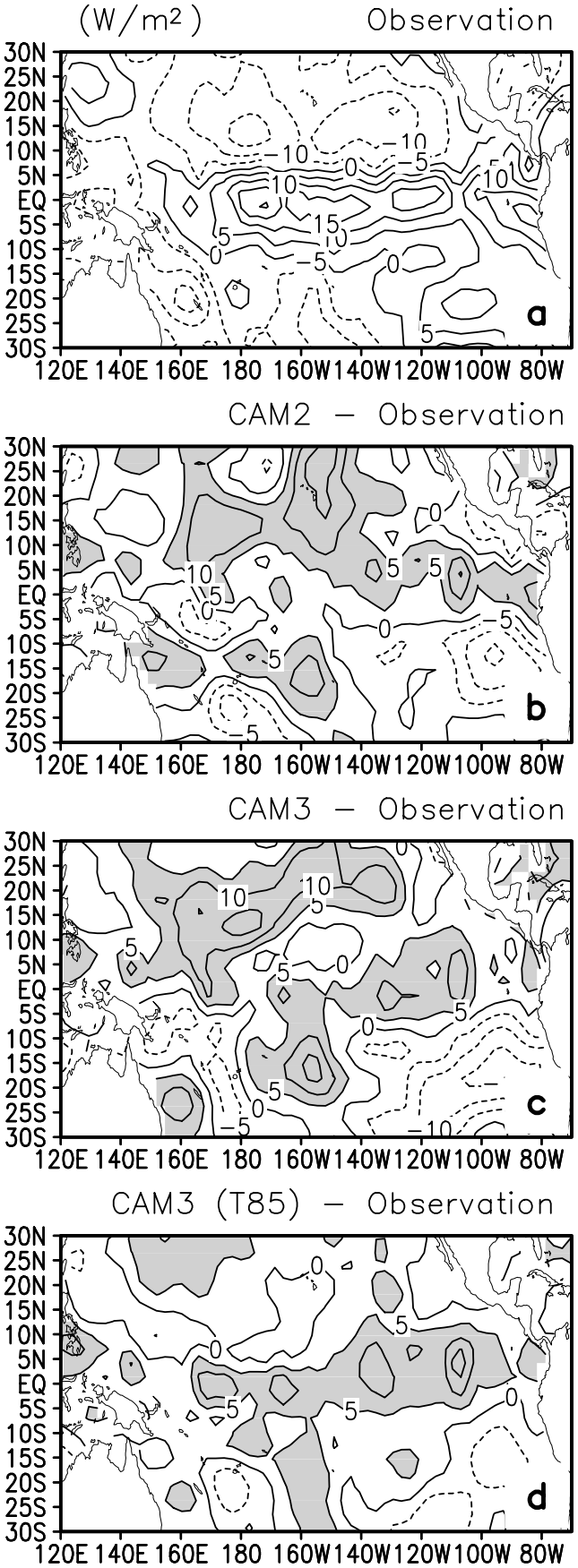

Figure 6. (a) Geographical distributions of the difference (April 1987 minus April 1985) in the greenhouse effect of water vapor (Ga) over the tropical Pacific from ERBE observations, (b) the difference between CAM2 and observations, (c) the difference between T42 CAM3 and observations, and (d) the difference between T85 CAM3 and observations.

that in the warm phase, the bias of the underestimate of Cl in the CAM2 and the T42 CAM3 is greatly improved in the T85 CAM3 over the central Pacific (Figure 14d).

[24] The changes in Cs from April 1985 to April 1987 for ERBE observations and models are shown in Figure 15. Consistent with previous studies [*Chou*, 1994; *Sun and Trenberth*, 1998], observations show a negative change over the equatorial Pacific owing to the more cloudiness causing an enhanced albedo cooling effect. The similarity of the observed pattern of the change in Cs and Cl but with the opposite sign (Figures 15a and 11a) indicates a near cancellation of the cloud forcing over the Pacific, however, this observed cancellation is not well captured in the NCAR models since the simulated changes in Cs exhibit a large unrealistic positive contribution especially over the region of El Niño warming in the CAM2 (Figure 15b). The unrealistic positive contribution over the eastern Pacific remains in the T85 CAM3, but the negative contribution over the central Pacific is overestimated by about 40 W m^{-2} (Figure 15d), this excessive cooling effect can also be found in the climatology (Figure 3h). We will discuss the cause of the model bias in Cs later in this study (see section 3.3). The same analysis is used to find out which phase during ENSO is the main error contributor to the simulated change in Cs (Figure 16). Interestingly, both the warm El Niño condition and cold La Niña condition are responsible for the biases. It can be seen clearly that the models show less negative contributions (shaded positive biases) during warm condition (Figures 16b–16d) and more negative contributions (shaded negative biases) during cold condition (Figures 16f–16h) compared to observations.

3.3. Regression Analysis

[25] The above analysis of the difference between April 1987 and April 1985 gives us a qualitative description of model's capability in simulating the response of greenhouse effect of water vapor and cloud radiative forcing to El Niño warming with the focus on April [*Chou*, 1994; *Soden*, 1997; *Sun and Trenberth*, 1998]. However, as demonstrated by *Soden* [1997], the greenhouse effect of water vapor is very sensitive to the month chosen and the difference also shows significant month-to-month variability in both sign and magnitude. To obtain a better understanding of how the greenhouse effect of water vapor and cloud radiative forcing over the region of El Niño warming evolve during the ERBE period, the time series of the interannual anomalies of observed and simulated Ga, Cl, and Cs is illustrated in Figure 17. It confirms that the main bias of simulated Ga and Cl stems from the warm El Niño condition in which Ga is overestimated in three models and Cl is underestimated in the CAM2 and the T42 CAM3 (Figures 17a and 17b). It can also be seen that the large bias of simulated Cs exists in both the warm condition and cold condition (Figure 17c), con-

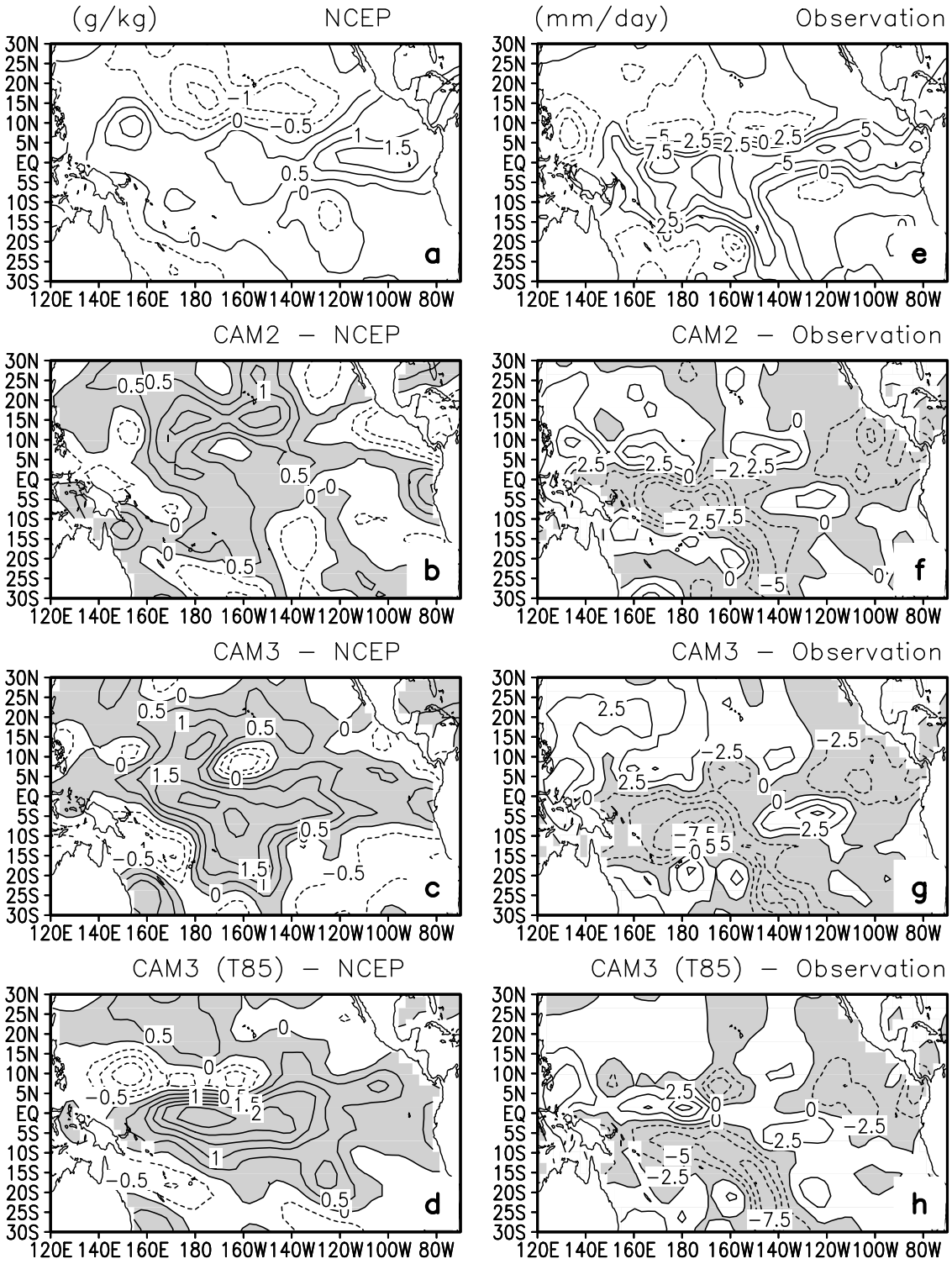

Figure 7. (a) Geographical distributions of the difference (April 1987 minus April 1985) in the specific humidity in the upper troposphere (500 hPa) over the tropical Pacific from the NCEP-NCAR reanalysis, (b) the difference between CAM2 and NCEP data, (c) the difference between T42 CAM3 and NCEP data, and (d) the difference between T85 CAM3 and NCEP data. Shown also are (e) the spatial patterns of the difference (April 1987 minus April 1985) in the precipitation from CMAP observations [*Xie and Arkin*, 1997], (f) the difference between CAM2 and observations, (g) the difference between T42 CAM3 and observations, and (h) the difference between T85 CAM3 and observations.

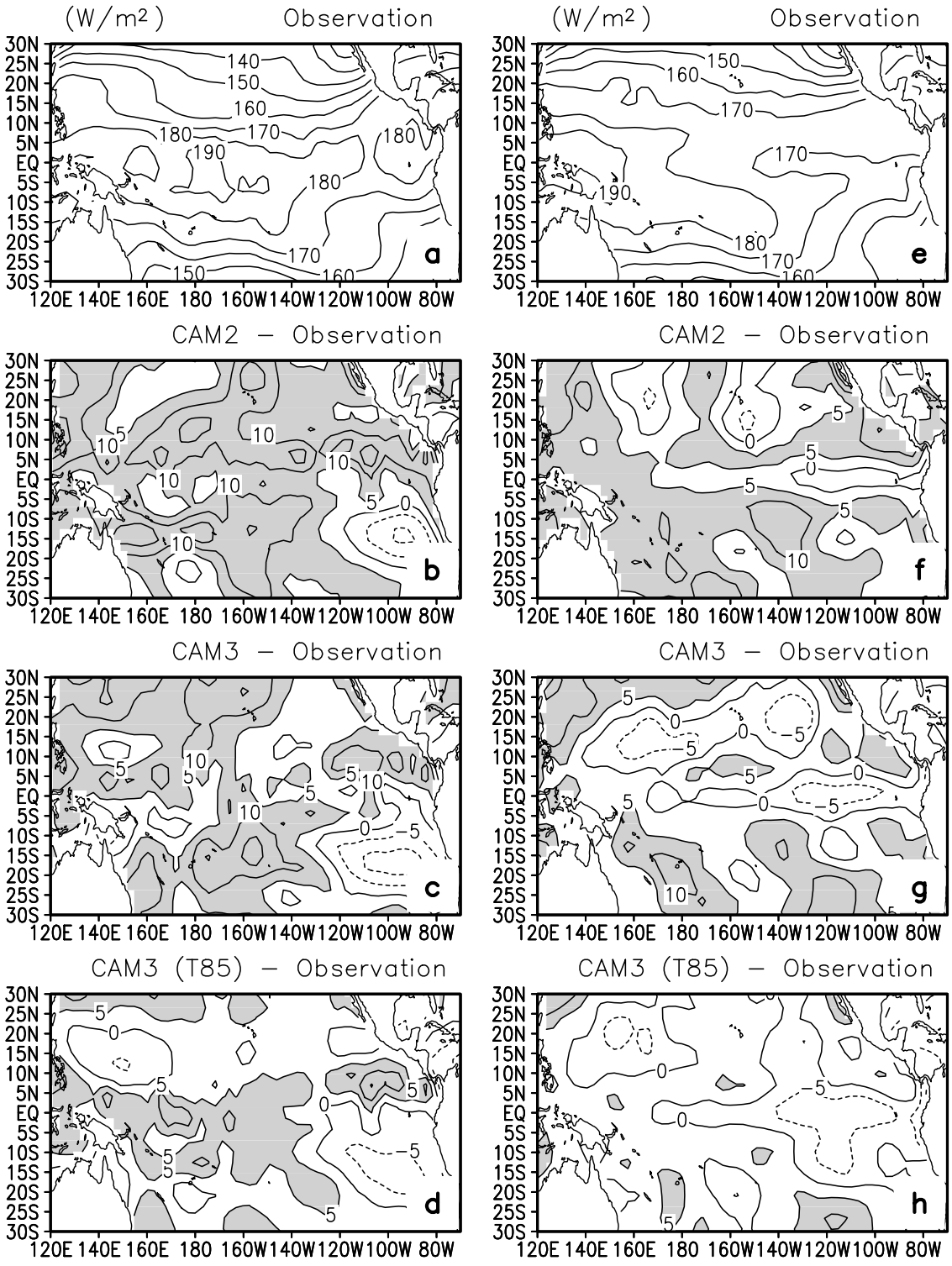

Figure 8. (a) Geographical distributions of the greenhouse effect of water vapor (Ga) from observations and the differences between (b) CAM2, (c) T42 CAM3, and (d) T85 CAM3 and observations in April 1987. (e–h) Corresponding observations and differences between three models and observations in April 1985, respectively.

sistent with previous discussion (Figure 16). Furthermore, the observed Cs shows an enhanced cooling effect in going from the cold La Niña to the warm El Niño and thus represents a negative response, but two of the three models tend to exhibit an enhanced warming effect and thus simulate an unreasonable positive response especially in the CAM2 (Figure 17c). To further quantify the responses, we linearly regress the time series of Ga, Cl and Cs shown

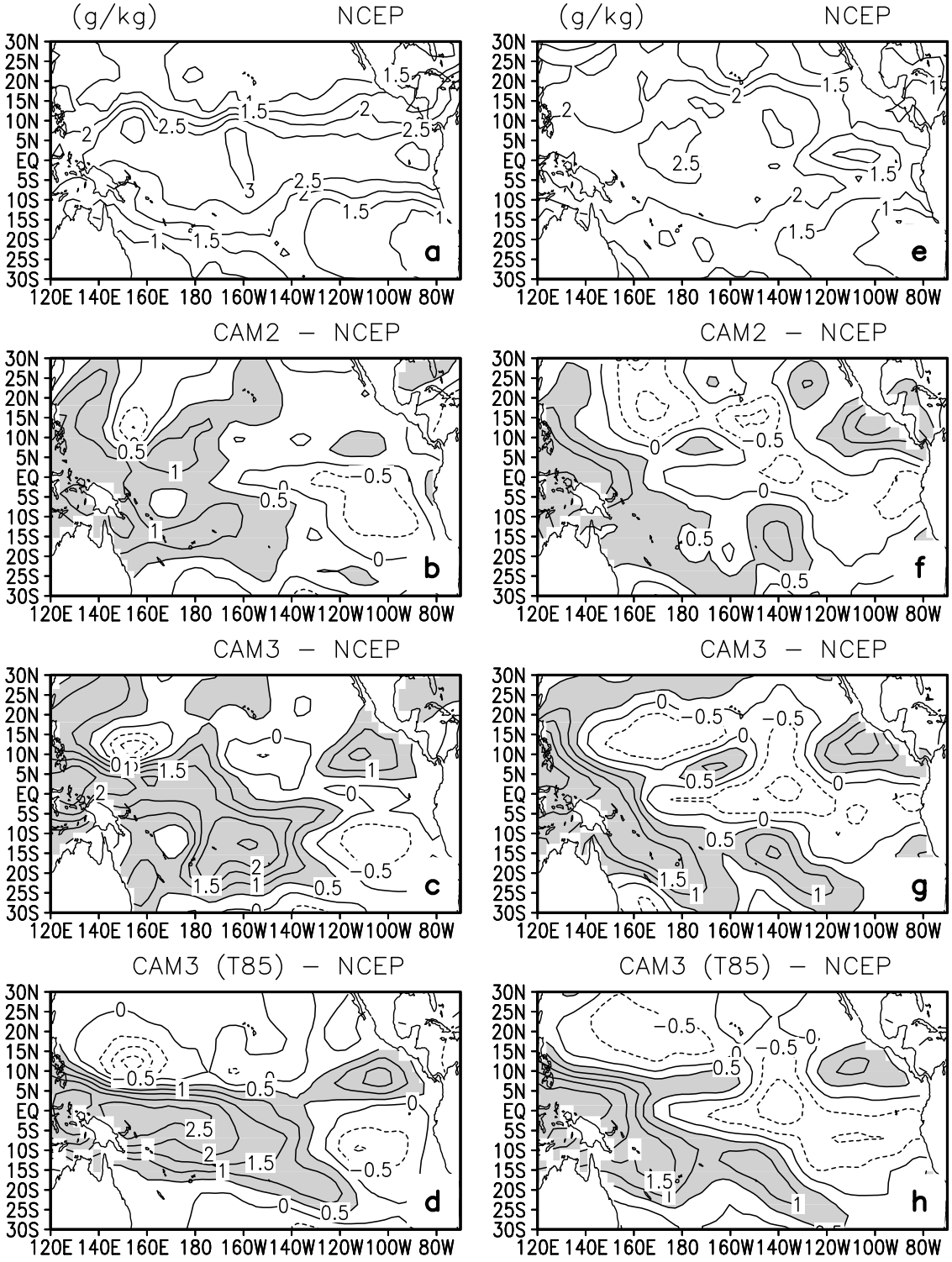

Figure 9. (a) Geographical distributions of the specific humidity in the upper troposphere (500 hPa) from NCEP reanalysis and the differences between (b) CAM2, (c) T42 CAM3, and (d) T85 CAM3 and NCEP reanalysis in April 1987. (e–h) Corresponding NCEP reanalysis and differences between three models and NCEP reanalysis in April 1985, respectively.

in Figure 17 against the underlying SST signal over the region of El Niño warming [*Sun et al.*, 2003] and the results are listed in Table 1. The numbers in Table 1 strengthen the impression that the positive response from Ga is overestimated in all three models, the positive response from Cl is underestimated in the CAM2 and the T42 CAM3, and the negative response from Cs is unreasonably simulated with the wrong sign in these two models. Specifically, the

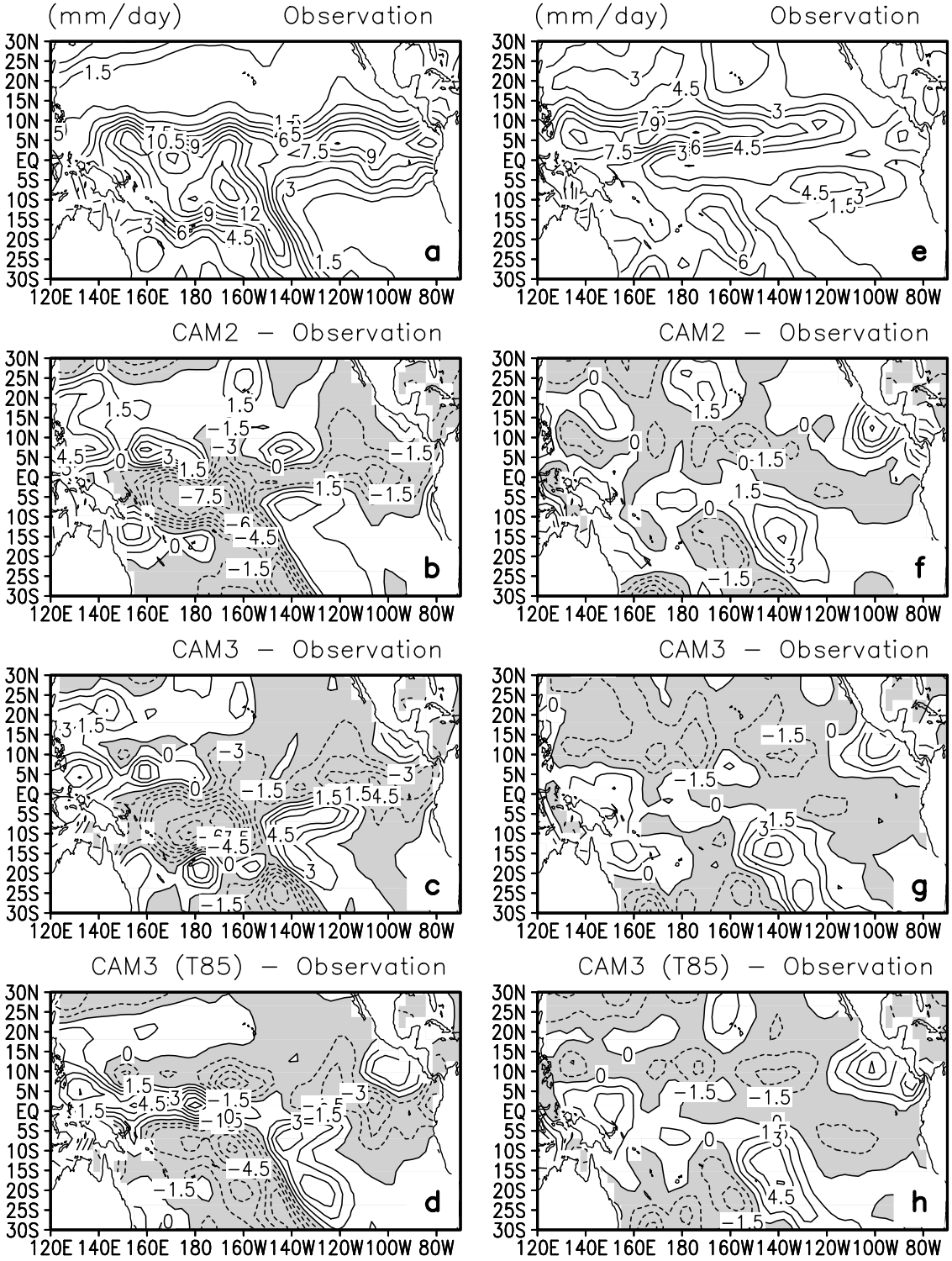

Figure 10. (a) Geographical distributions of precipitation from CMAP observations [*Xie and Arkin*, 1997] and the differences between (b) CAM2, (c) T42 CAM3, and (d) T85 CAM3 and CMAP observations in April 1987. (e–h) Corresponding observations and differences between three models and observations in April 1985, respectively.

response from Ga is overestimated by 28%, 31% and 36% in the CAM2, the T42 CAM3 and the T85 CAM3, respectively. The response from Cl is underestimated by 37% in the CAM2 but it is a little bit improved and the underestimation is reduced to 34% in the T42 CAM3, while the response from Cl in the T85 CAM3 is comparable to the observed value. The most significant bias exists in the simulation of response from Cs. The observations show a

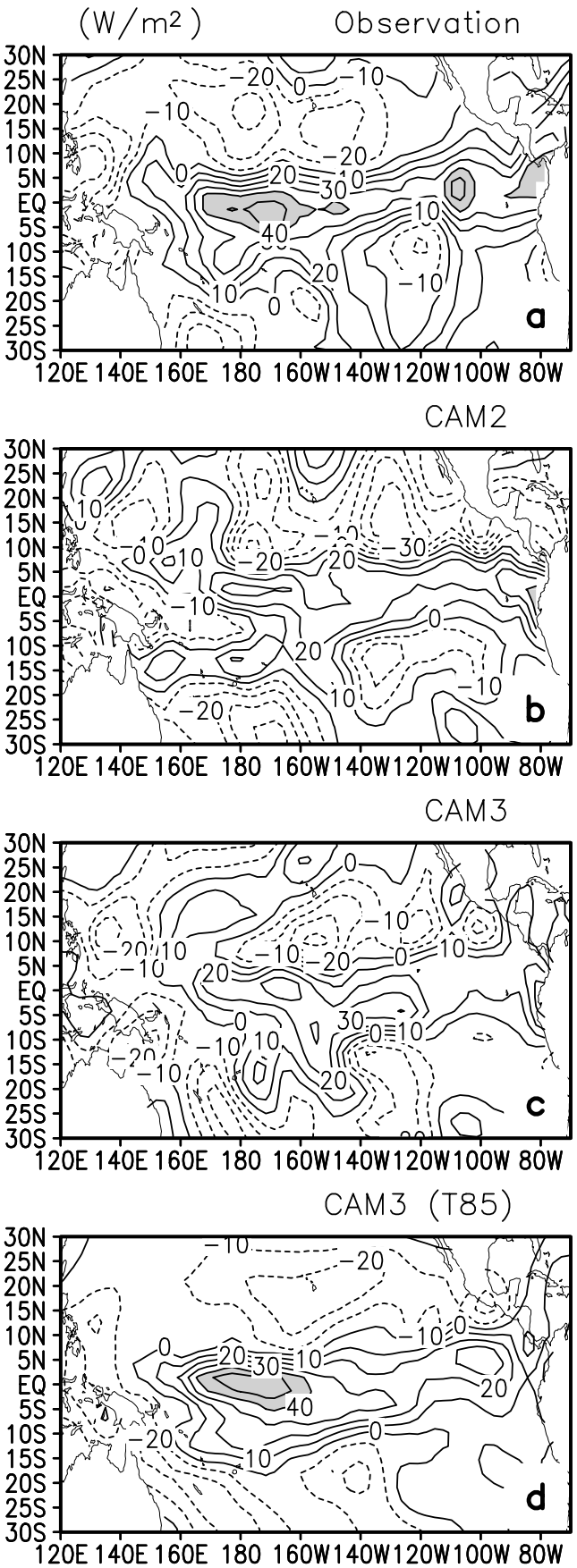

Figure 11. (a) Geographical distributions of the difference (April 1987 minus April 1985) in the cloud longwave radiative forcing (Cl) over the tropical Pacific from ERBE observations, (b) CAM2, (c) T42 CAM3, and (d) T85 CAM3.

negative response from Cs (-7.79 W m^{-2} K^{-1}) whereas the CAM2 presents a positive response (3.41W m^{-2} K^{-1}). The magnitude of the bias in the response from Cs is somewhat reduced in the T42 CAM3 but still kept the wrong sign (1.04 W m^{-2} K^{-1}), the T85 CAM3 gets the correct sign but underestimates the negative response from Cs by about 34%.

[26] To gain a deep insight into the numbers summarized in Table 1, the spatial pattern of the response of Ga, Cl, and Cs to El Niño warming is conducted by linearly regressing interannual variations of the corresponding fluxes in every grid point against the same SST signal, following the same way used by *Sun et al.* [2003]. Figure 18 shows the geographical distribution of the response of Ga to El Niño warming. It can be seen that the observed response from Ga is characterized by a positive contribution over the tropical Pacific with the maximum locating in the central Pacific (Figure 18a), the three models can reproduce this observed positive response from Ga including the location of the maximum. However, the magnitude of response is somewhat overestimated in three models (Figures 18b–18d), and this overestimation is more significant in the T85 CAM3, in agreement with the results shown in Table 1. The spatial pattern of the response of atmospheric moisture (specific humidity) to El Niño warming from observations and models is shown in Figure 19. Consistent with the difference between April 1987 and April 1985 (Figures 7a–7d), the response from atmospheric moisture in the upper tropical troposphere (500 hPa) remains the main contributor to the bias of response from Ga (Figures 19a–19d), the stronger response of atmospheric moisture over the equatorial central Pacific in the T85 CAM3 than in other two models indicates the more effectiveness of greenhouse trapping of water vapor and thus leads to the stronger overestimation of response from Ga in the T85 CAM3 over that region (Figure 18). A close look of Figure 19 also reveals a weaker water vapor response in the T85 CAM3 than in the T42 CAM3 over the equatorial eastern Pacific, consistent with what we see from Figure 18: The T85 CAM3 has a slightly weaker response of Ga relative to the T42 CAM3 over the equatorial eastern Pacific. Compared to NCEP reanalysis, the water vapor response in the upper troposphere is overestimated by 7%, 19% and 19% in the CAM2, the T42 CAM3 and the T85 CAM3 over the region of El Niño warming (160°–290°E, 5°S–5°N), respectively (Table 2). It is noted that the atmospheric moisture response in the low tropical troposphere (850 hPa) is small, suggesting that the water vapor in the low tropical troposphere may not be a significant error source of Ga (Figures 19e–19h).

[27] The same analysis is applied to Cl and Cs (Figure 20). Similar to the pattern of Ga (Figure 18a), the observed response of Cl to El Niño warming is dominated by an enhanced positive contribution with the maximum centering at the equatorial central Pacific (Figure 20a). The models

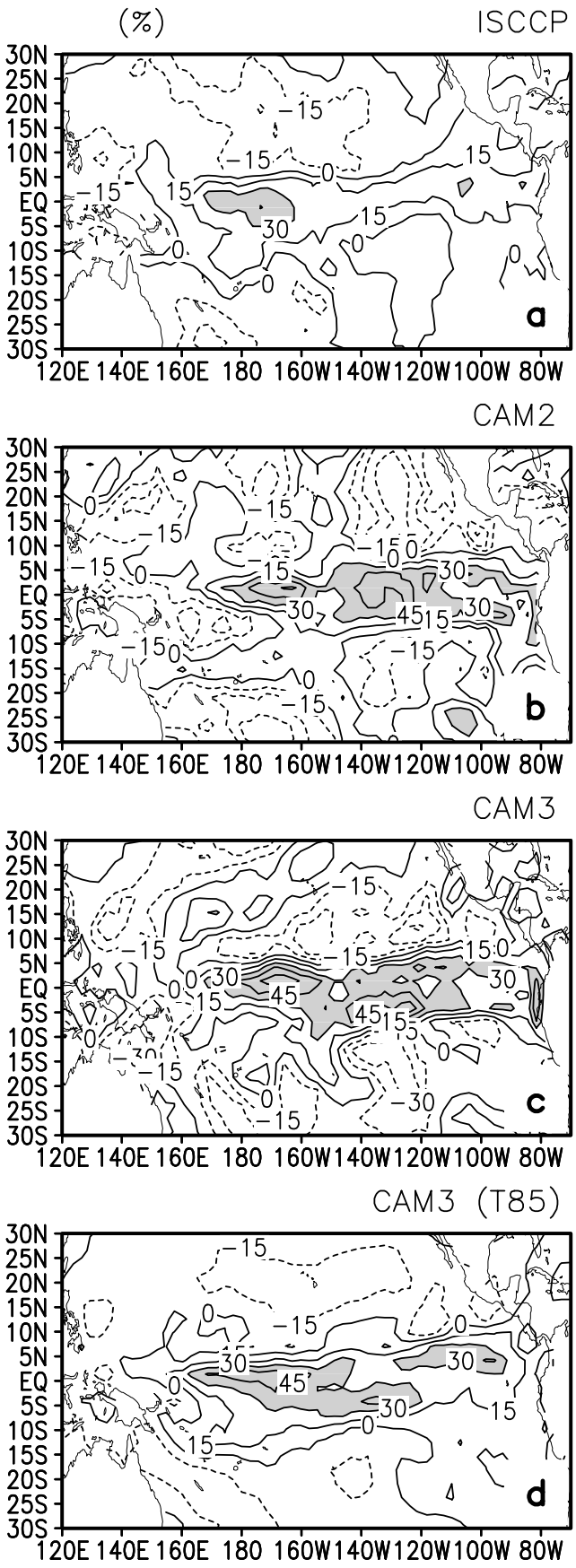

are found to be capable of reproducing this positive response. However, the magnitude is weakened in the CAM2 and the T42 CAM3 (Figures 20b and 20c), but this weakness is removed in the high-resolution model: The T85 CAM3 can well reproduce the observed values (Figure 20d). The simulated maximum center seems to be shifted eastward slightly, especially in two CAM3 models. The observed response of Cs shows a negative response contrary to that of Cl (Figure 20e), while the CAM2 fails to reproduce this negative response and presents an overly positive contribution dominating in the eastern Pacific (Figure 20f). Two CAM3 models appear to have some improvements in the simulation over the central Pacific, although they still have the same problem as the CAM2 in the simulation over the eastern Pacific (Figures 20g and 20h). The negative response from Cs over the central Pacific is about 10 W m^{-2} K^{-1} underestimated in the T42 CAM3 (Figure 20g), but it is about 10 W m^{-2} K^{-1} overestimated in the T85 CAM3 (Figure 20h). This excessive response of Cs in the T85 CAM3 over the central Pacific is consistent with the large difference in Cs between April 1987 and April 1985 over that region (Figure 15d).

[28] Shown in Figure 21 is the spatial pattern of the response of high cloud cover from observations and three models. The simulated maximum center of the high cloud response in the CAM2 and the T42 CAM3 obviously shifts eastward (Figures 21b and 21c), leading to a weaker response over the central Pacific, where the observed response of high cloud cover shows a dominant effect on that of Cl (see Figures 21a and 20a). This may contribute to the underestimation of Cl response in these two models. The slightly improved response from Cl in the T42 CAM3 than in the CAM2 (Table 1) could be due to the improvement of the maximum center of high cloud response moving from 150°W in the CAM2 to 160°W in the T42 CAM3, which is closer to the observed (Figures 21b and 21c). Interestingly, compared to the T42 CAM3, the response of high cloud cover in the T85 CAM3 is almost unchanged (Figures 21c and 21d). A quantitative measure of the high cloud response is listed in Table 2. The results show that the responses of high cloud cover in three models are very comparable to each other averaged over the region of El Niño warming. We notice that the high cloud cover in the climatology in the CAM2 is three times as large as the observed (Figures 4a and 4b). This positive bias exists in both the warm and cold phases (Figures 13b and 13f). Because the cloud cover in the cold phase is already so high, and the cloud cover is bounded by 100%, the response of high cloud cover to El Niño warming is not much enhanced (Figures 21a and 21b).

[29] The middle and low cloud cover play a vital role in affecting cloud shortwave forcing [*Hartmann et al.*, 1992]. It is found that in relation to the CAM2, the improvement of response from Cs over the central Pacific in two CAM3 models (Figures 20g and 20h) is associated with an enhanced middle cloud response, which is comparable to the

Figure 12. (a) Geographical distributions of the difference (April 1987 minus April 1985) in the high cloud amount over the tropical Pacific from ISCCP observations, (b) CAM2, (c) T42 CAM3, and (d) T85 CAM3.

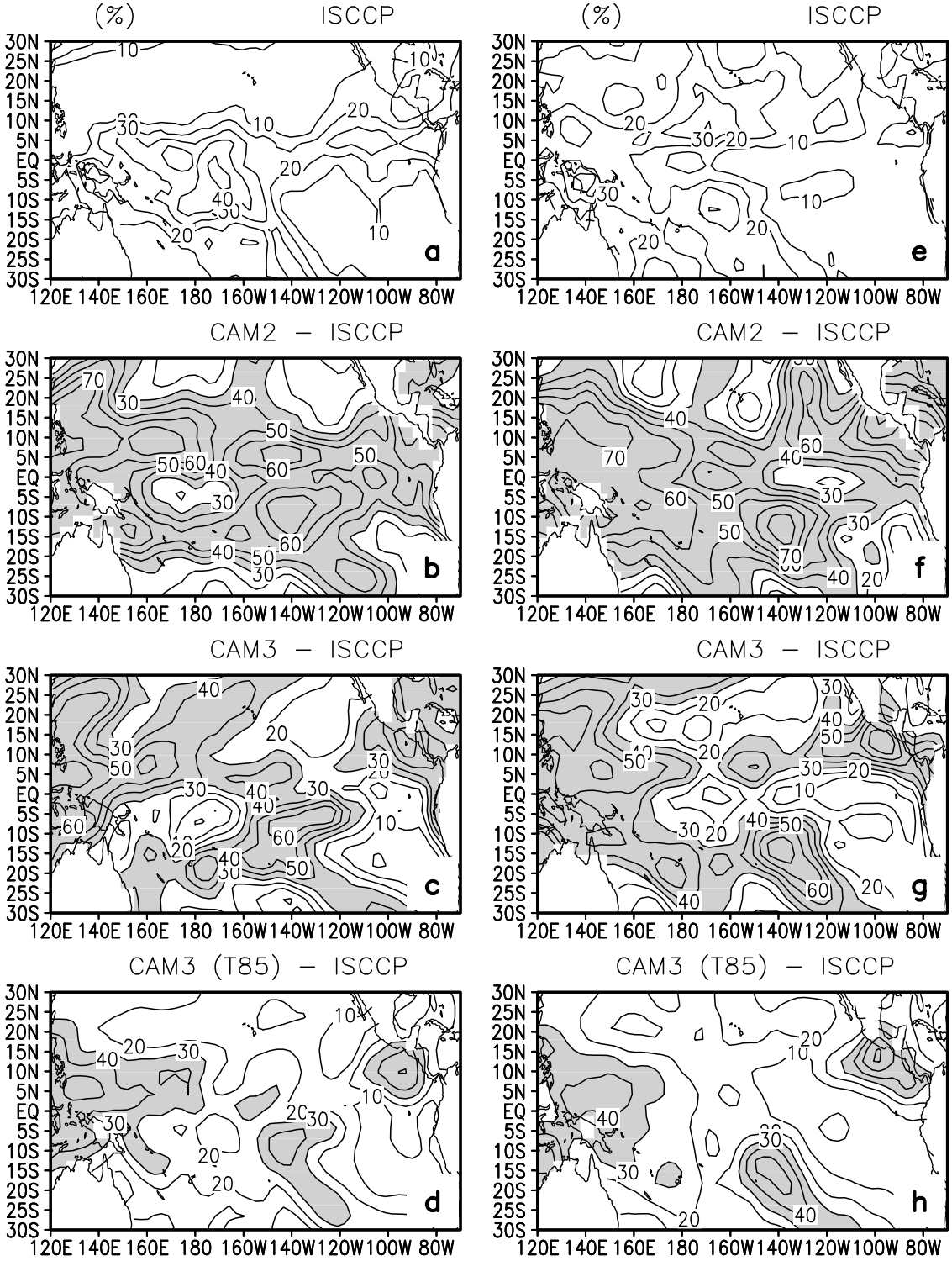

Figure 13. (a) Geographical distributions of the high cloud amount from ISCCP observations and the differences between (b) CAM2, (c) T42 CAM3, and (d) T85 CAM3 and ISCCP observations in April 1987. (e–h) Corresponding observations and differences between three models and observations in April 1985, respectively.

observed in the T42 CAM3 (Figure 22c) and somewhat overestimated in the T85 CAM3 (Figure 22d). The stronger response of middle cloud cover in the T85 CAM3 is consistent with the modeled stronger response of Cs over the central Pacific (Figure 20h), and may also contribute to the improvement of response of Cl in that region as middle level clouds contribute effectively to both the reflection of the solar radiation and the trapping of longwave radiation

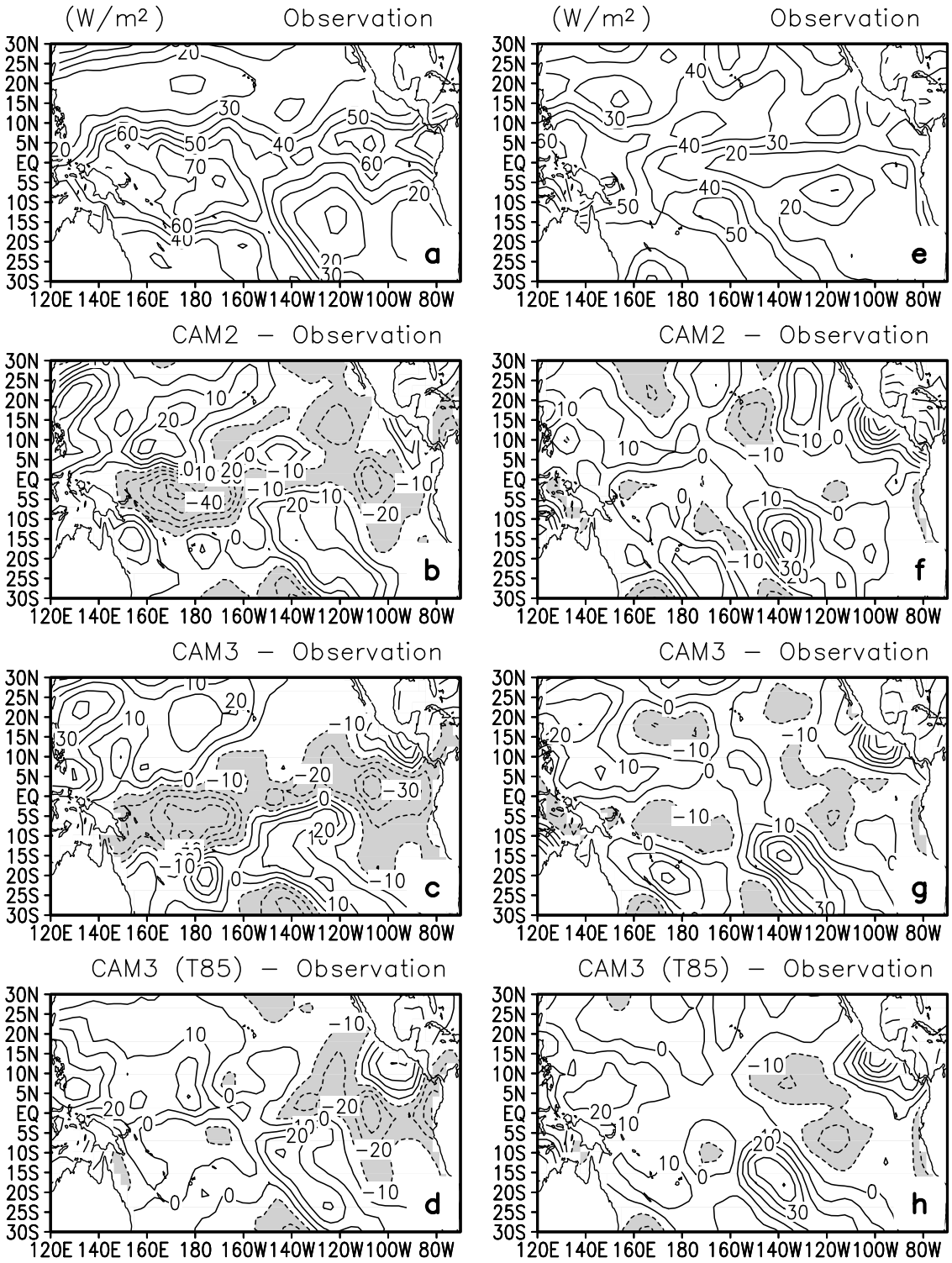

Figure 14. (a) Geographical distributions of the cloud longwave radiative forcing (Cl) from ERBE observations and the differences between (b) CAM2, (c) T42 CAM3, and (d) T85 CAM3 and ERBE observations in April 1987. (e–h) Corresponding observations and differences between three models and observations in April 1985, respectively.

(Figure 20d). However, the unrealistic large negative response of low cloud (Table 2) is hardly changed over the eastern Pacific in three models (Figures 22f–22h), which may contribute to the common problem that the unreasonable large positive response from Cs exists in three models over that region (Figures 20f–20h).

[30] Both the CAM2 and two CAM3 models diagnose the low-level marine stratocumulus clouds based on the *Klein*

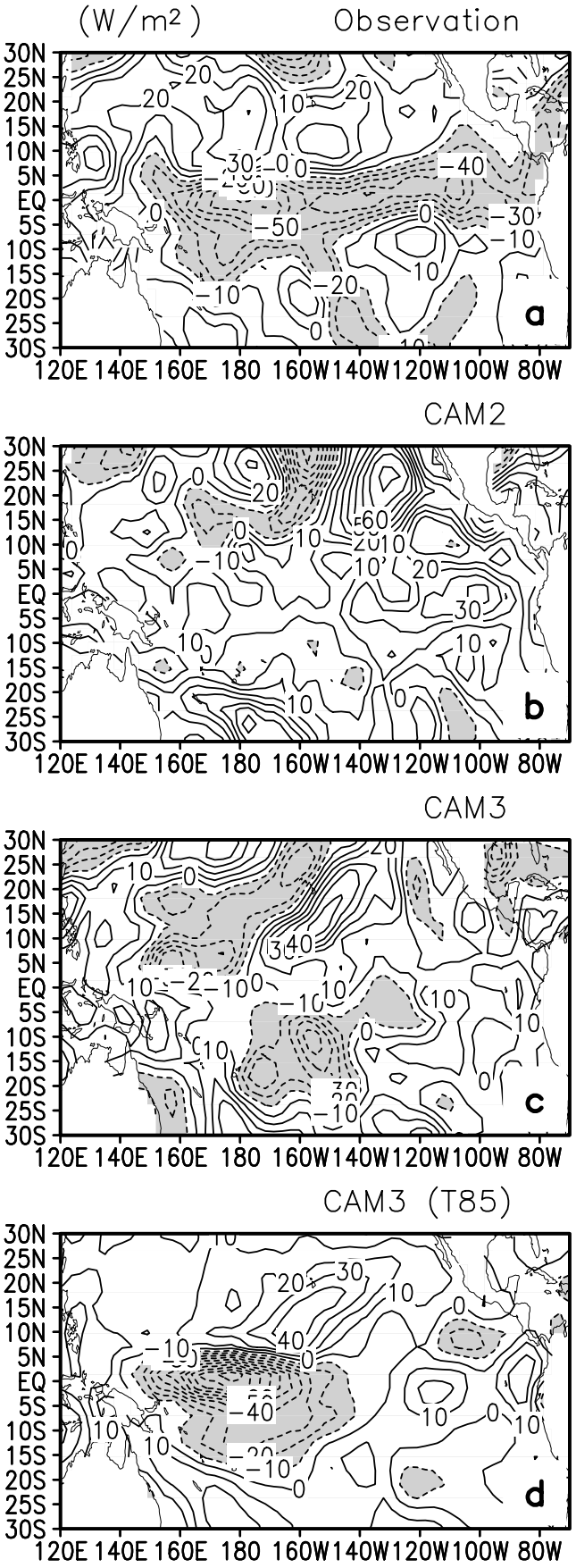

and Hartmann [1993] scheme. The scheme uses an empirical relationship between marine stratocumulus cloud fraction (Cst) and the potential temperature difference between 700 mbar and surface [*Collins et al.*, 2003, 2004],

$$\mathrm{Cst} = \min\{1., \max[0., 0.057(\theta_{700} - \theta_S) - 0.5573]\} \qquad (4)$$

θ_{700} and θ_S are the potential temperatures at 700 mbar and the surface, respectively. Figure 23 shows the annual mean low cloud amount from surface observation [*Dai and Trenberth*, 2004], the marine stratocumulus cloud amount derived using the above diagnostic scheme (equation (4)) with observed potential temperature, and with simulated potential temperature from three models. The low cloud pattern from surface observation (Figure 23a) is in good agreement with that from ISCCP data (Figure 5e), including the maximum over the Northern Pacific in the midlatitudes and the minimum over the equatorial southeastern Pacific. The pattern of marine stratocumulus cloud amount derived using the *Klein and Hartmann* [1993] scheme with the simulated potential temperature from three models (Figures 23c–23e) is also very similar to that of the low cloud amount output directly from three AMIP runs of the NCAR model, suggesting that the low-level cloud amount is dominated by the contribution of marine stratocumulus cloud amount. However, this empirical relationship fails to reproduce the observed minimum center over the equatorial southeastern Pacific where the wrong response of low cloud originates, even with the observed surface temperature and the NCEP-NCAR reanalysis 700 mbar temperature (both translated into potential temperature at the 1000 mbar reference) (Figure 23b). Therefore it is possible that this simple empirical relationship has deficiency in reproducing the principle feature of low cloud over the equatorial eastern Pacific and may not be adequate in simulating the response of the region's low cloud to ENSO.

4. Summary and Discussions

[31] In this study, we have carried out a detailed analysis of the response of water vapor and clouds to El Niño warming over the tropical Pacific in the NCAR Community Atmosphere Model (CAM2 and CAM3 at T42 and at T85 resolutions). We first examine the differences in the water vapor and clouds fields between April 1987 (an El Niño year) and April 1985 (a non-El Niño year). We further quantify the response of water vapor and clouds by linearly regressing the interannual variations of the corresponding fields to the underlying SST. The results show that in general, the changes made to the parameterizations of clouds from CAM2 to CAM3 improve the response of clouds to El Niño warming. By comparing the results from CAM3 at T85 resolution with those from CAM3 at the standard T42 resolution, we also find that a higher horizon-

Figure 15. (a) Geographical distributions of the difference (April 1987 minus April 1985) in the cloud shortwave radiative forcing (Cs) over the tropical Pacific from ERBE observations, (b) CAM2, (c) T42 CAM3, and (d) T85 CAM3.

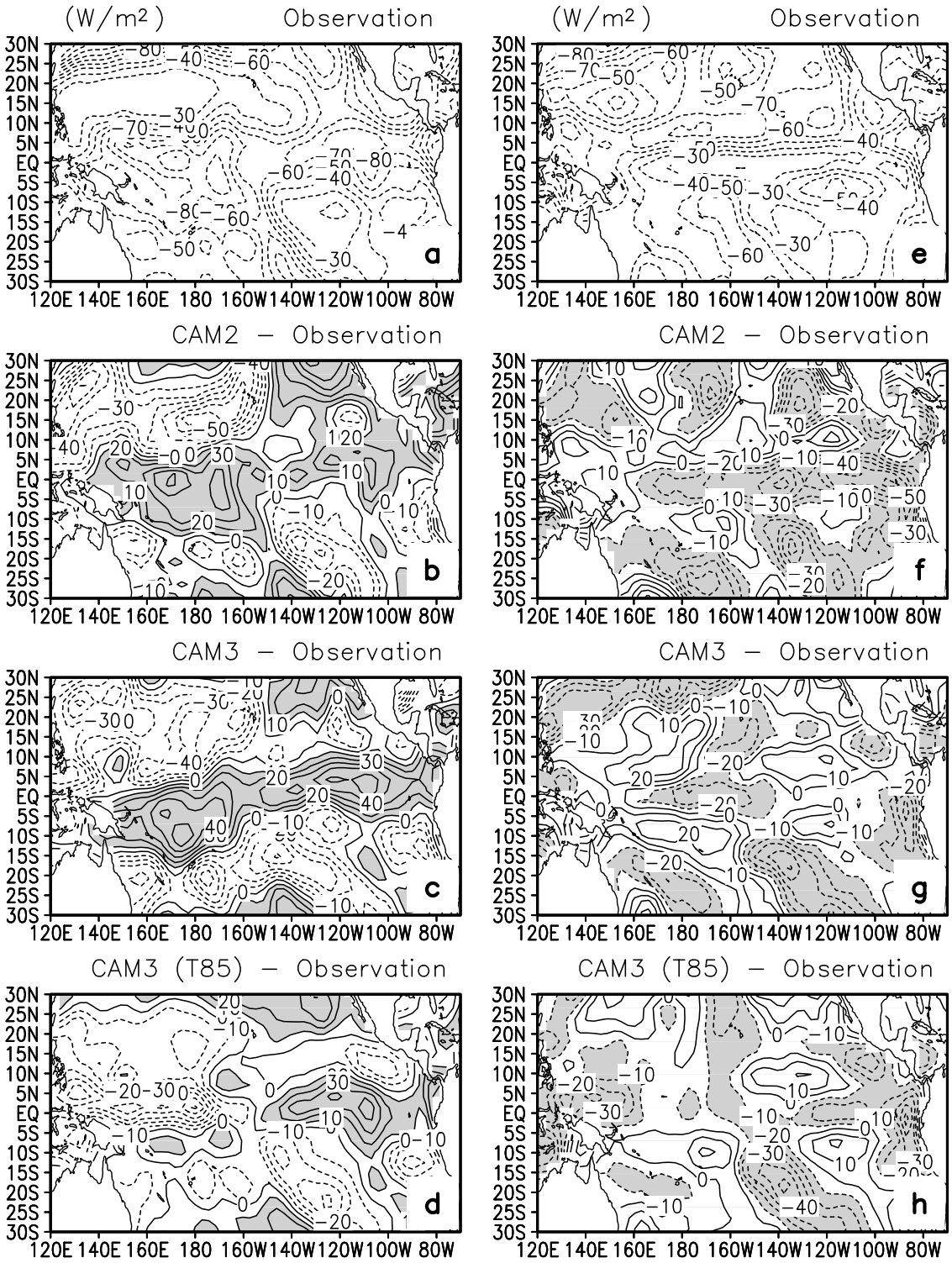

Figure 16. (a) Geographical distributions of the cloud shortwave radiative forcing (Cs) from ERBE observations and the differences between (b) CAM2, (c) T42 CAM3, and (d) T85 CAM3 and ERBE observations in April 1987. (e–h) corresponding observations and differences between three models and observations in April 1985, respectively.

tal resolution results in a better simulation of the response of clouds to El Niño warming. However, these changes in the parameterizations and resolutions in the NCAR models result in no improvements in the simulation of water vapor response to El Niño warming. The overestimate of the response of the greenhouse effect of water vapor persists in all three versions and there is evidence that this overestimate is due to a moist bias in the upper troposphere. The

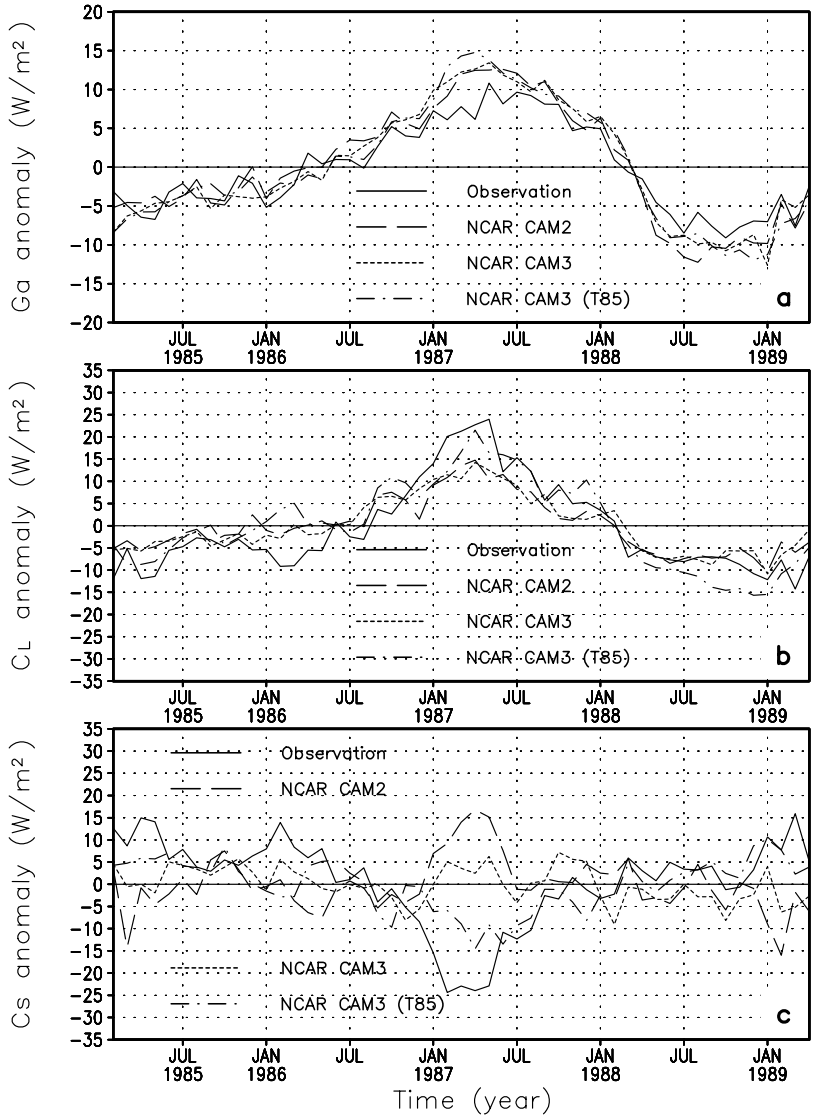

Figure 17. (a) Time series of interannual variations of greenhouse effect of water vapor (Ga), (b) cloud longwave radiative forcing (Cl), and (c) cloud shortwave radiative forcing (Cs) averaged over the region of El Niño warming (160°–290°E, 5°S–5°N) for ERBE observations (solid line), CAM2 (long-dashed line), T42 CAM3 (short-dashed line), and T85 CAM3 (dot-dashed line) simulations.

cloud cover in the upper troposphere in all models is much greater than that seen in ISCCP. All models underestimate changes in precipitation to changes in SST, particularly in regions with warm SST.

Table 1. Responses From Greenhouse Effect of Water Vapor and Cloud Radiative Forcing to ENSO Forcing Over the Region of El Niño Warming (160°–290°E, 5°S–5°N)[a]

Response, W m^{-2} K^{-1}	Observation, CAM2, CAM3, CAM3 (T85)
$\frac{\partial(G_a)}{\partial T}$	6.37 ± 0.23, 8.17 ± 0.31, 8.33 ± 0.27, 8.65 ± 0.29
$\frac{\partial(C_L)}{\partial T}$	9.81 ± 0.88, 6.20 ± 0.49, 6.49 ± 0.47, 10.21 ± 0.60
$\frac{\partial(C_S)}{\partial T}$	−7.79 ± 1.23, 3.41 ± 0.92, 1.04 ± 0.64, −5.15 ± 0.62

[a]The responses are obtained through a linear regression using the interannual variations of the SST and the corresponding fluxes over the region of El Niño warming, the same as done by *Sun et al.* [2003].

Table 2. Responses of Water Vapor and Cloud Cover to ENSO Forcing Averaged Over the Region of El Niño Warming (160°–290°E, 5°S–5°N)[a]

Response, % K^{-1}	Observation, CAM2, CAM3, CAM3 (T85)
Percentage response of specific humidity at 500 hPa	18.5,[b] 25.7, 37.4, 37.5
Percentage response of specific humidity at 850 hPa	4.0,[b] 3.2, 2.8, 4.7
Response of high cloud cover	5.7,[c] 8.8, 8.8, 9.1
Response of middle cloud cover	5.1,[c] 1.8, 4.7, 6.4
Response of low cloud cover	3.8,[c] −3.7, −3.5, −2.9

[a]Data used for the calculations here are the same as those used for obtaining Figures 19, 21, and 22.
[b]NCEP [*Kalnay et al.*, 1996].
[c]ISCCP [*Rossow and Schiffer*, 1999].

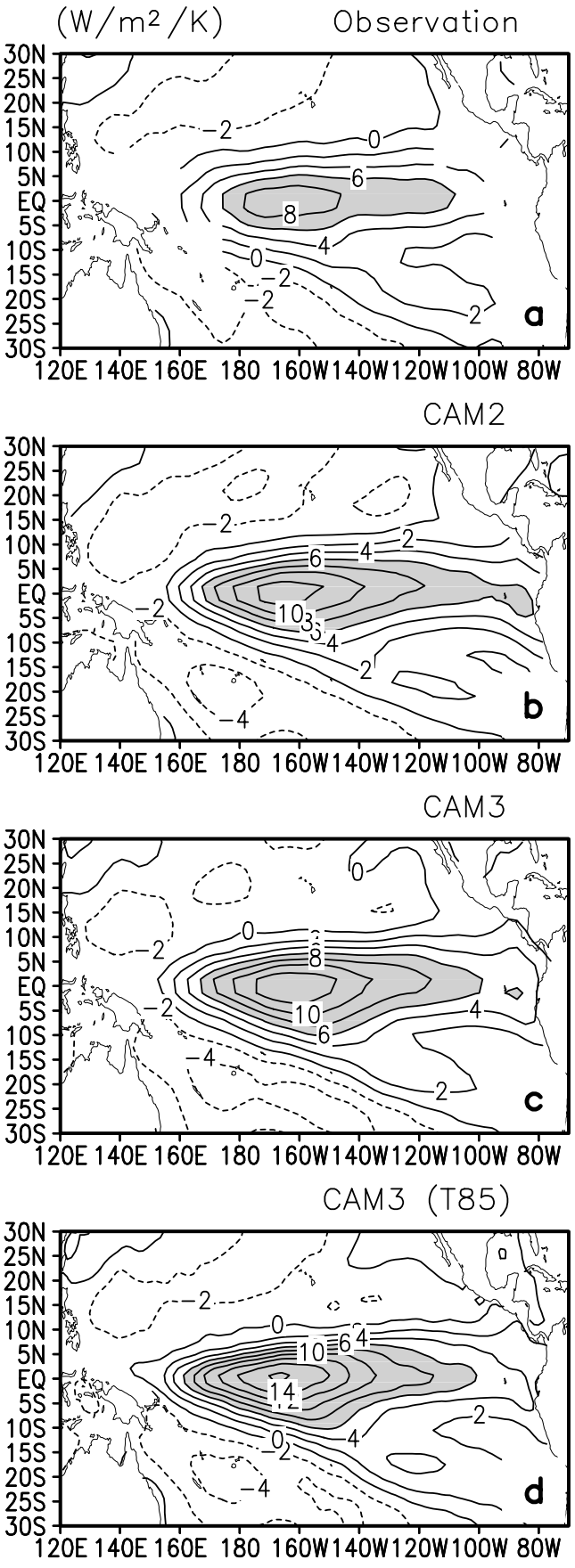

[32] Averaged over the region of El Niño warming, the positive response from Ga in the models is overestimated by about 28% in the CAM2 and about 36% in the T85 CAM3. This overestimation of response from Ga mainly comes from the bias in the warm El Niño condition. Consistent with the stronger response from Ga in three models, we find a greater response of atmospheric moisture content (e.g., specific humidity) in the upper troposphere in the model than that indicated in NCEP reanalysis. The overestimation of the response of atmospheric moisture ranges from 7% in the CAM2 to 19% in the T85 CAM3. The three models use the same deep moist convection parameterization scheme [*Zhang and McFarlane*, 1995], but the intensity of response of deep convection (measured by precipitation amount) to El Niño warming in the models is found to be surprisingly smaller than observations. *Zhang and McFarlane* [1995] convection scheme does not include convective inhibition induced by a stable boundary layer or descending large-scale motion. Instead, the scheme allows free convection whenever CAPE is above 75 J kg^{-1}. Consequently, the deep moist convection occurs too frequently [*Dai and Trenberth*, 2004]. The deep convection in the models may have a lower precipitation efficiency than that in observations. Whether this low precipitation efficiency is responsible for the excessive response of atmospheric moisture in the upper troposphere from the NCAR models needs to be explored. In this connection, it is worth noting that a recent study by *Xie et al.* [2004] implements a revised convection triggering mechanism in the CAM2. This new triggering mechanism introduces a dynamical constraint on the initiation of convection and requires a positive contribution from the large-scale advection of temperature and moisture to the existing positive CAPE for model convection to start. They found that the modified triggering mechanism in the CAM2 has led to less convection and a reduction in the overestimation of the upper tropospheric moisture (500 hPa). However, their analysis focused on the CAM2 results from short-range weather forecasts. An evaluation of the effect of modified convection triggering mechanism on the climate simulations by the CAM2 and CAM3 is not yet conducted.

[33] The CAM2 and T42 CAM3 both underestimate the response of Cl to El Niño warming. Both models have adequate response in cloud cover in the upper troposphere, suggesting that there are serious problems with optical properties of clouds. The shift of the maximum center of high cloud response is also responsible for the biases in Cl in the models. The T85 CAM3 has a stronger response in Cl, following a stronger response in middle level cloud cover. The related high cloud amount climatology is found to be excessively high over the deep convection region in

Figure 18. (a) Response of the greenhouse effect of water vapor (Ga) to El Niño warming from observations, (b) CAM2, (c) T42 CAM3, and (d) T85 CAM3. Shown are regression coefficients obtained by linearly regressing the greenhouse effect of water vapor at each grid point against the underlying SST averaged over the region of El Niño warming (160°–290°E, 5°S–5°N). The interannual variations of Ga over the ERBE period are used for the calculations.

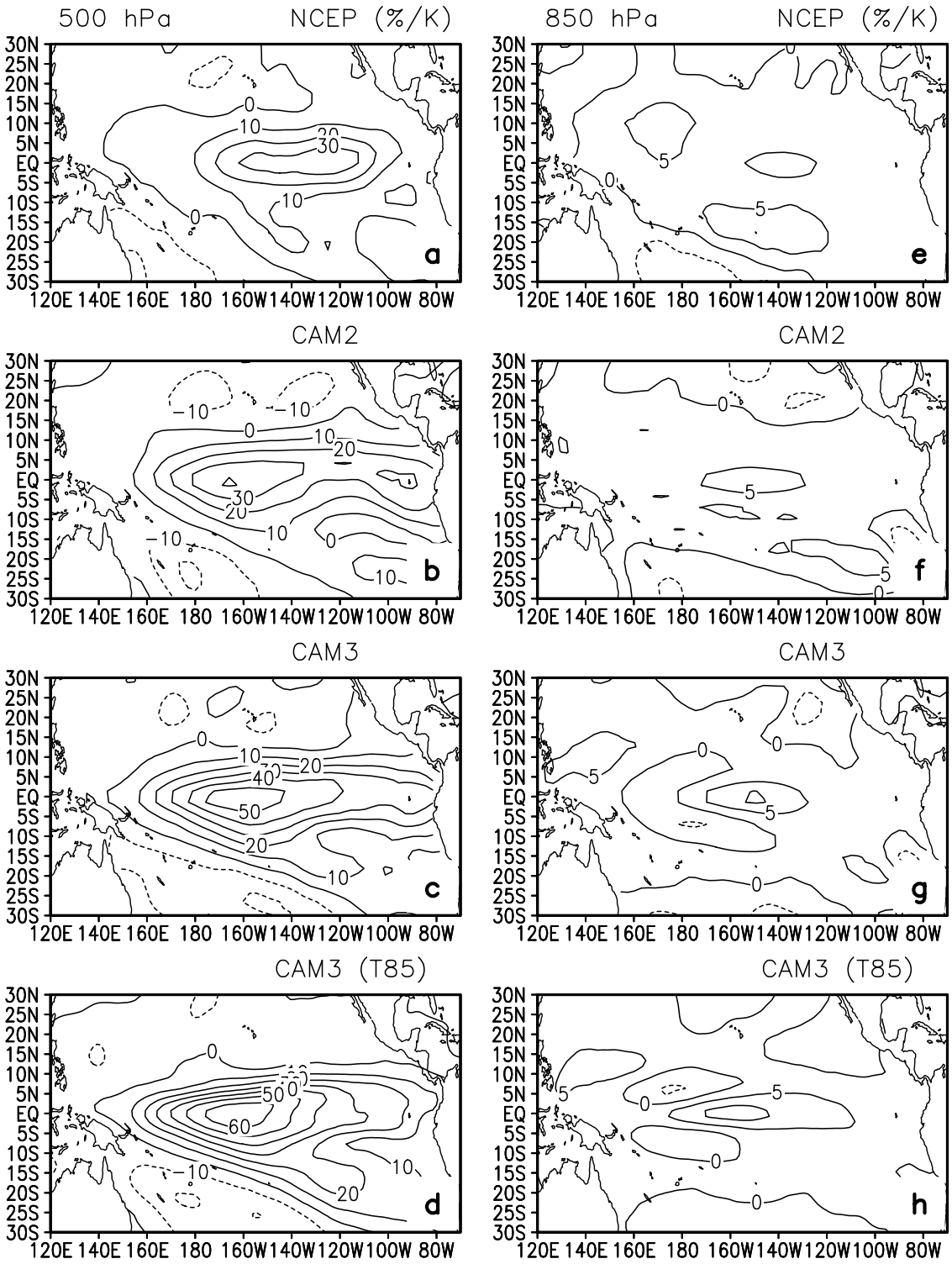

Figure 19. Percentage response of the specific humidity in (a–d) the upper troposphere (500 hPa) and in (e–h) the low troposphere (850 hPa) to El Niño warming from the NCEP-NCAR reanalysis, CAM2, T42 CAM3, and T85 CAM3. Shown are regression coefficients divided by the respective climatology. The regression coefficients are obtained by linearly regressing the specific humidity at each grid point against the underlying SST averaged over the region of El Niño warming (160°–290°E, 5°S–5°N). The interannual variations of specific humidity over the ERBE period are used for the regression calculations.

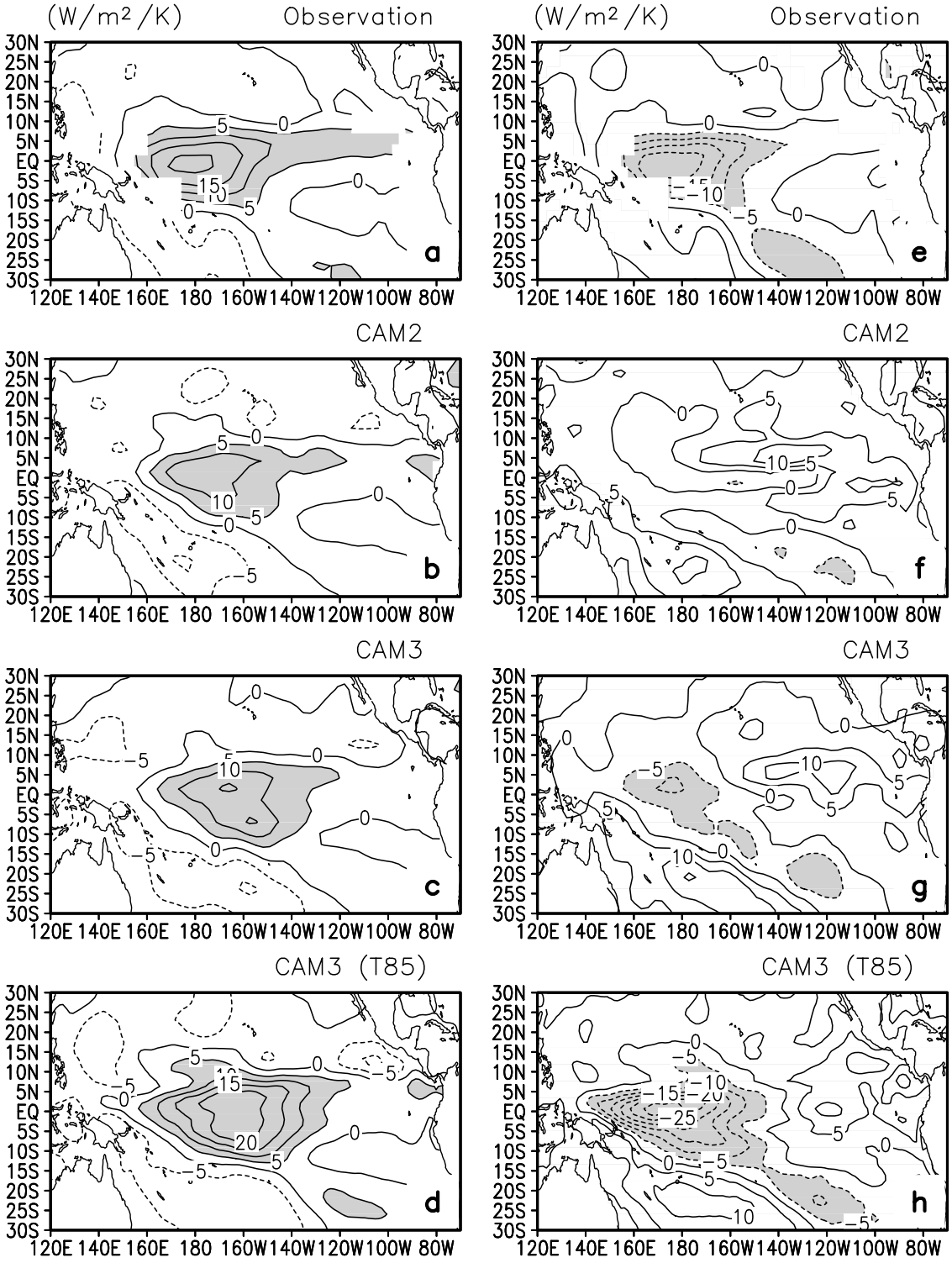

Figure 20. Response of (a–d) the cloud longwave forcing (Cl) and (e–h) the cloud shortwave forcing (Cs) to El Niño warming from ERBE observations, CAM2, T42 CAM3, and T85 CAM3. Shown are regression coefficients obtained by linearly regressing Cl and Cs at each grid point against the underlying SST averaged over the region of El Niño warming (160°–290°E, 5°S–5°N). The interannual variations of Cl and Cs over the ERBE period are used for the calculations.

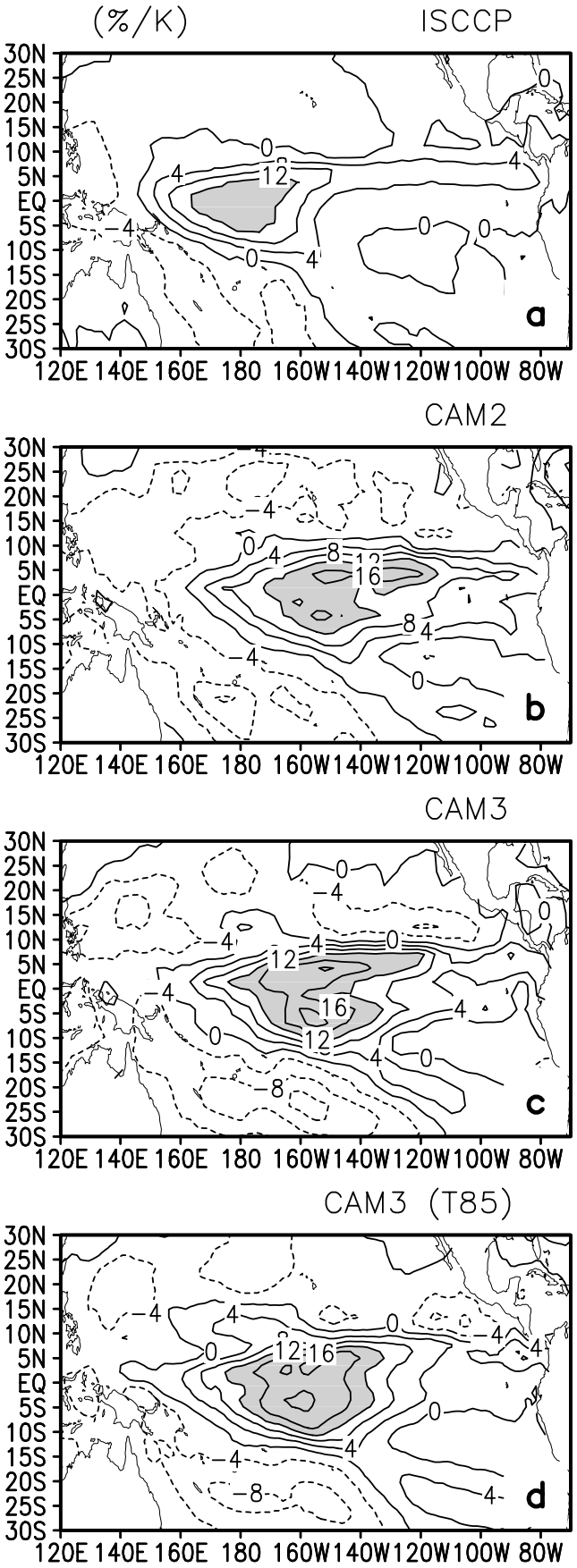

three models, due to the overestimation of cloud cover in both warm and cold phases. This overestimation of high cloud amount in the models may be due to the deficiency of too frequent convection occurrence. The study of *Xie et al.* [2004] have shown that their new triggering mechanism also substantially reduced the overestimation of the high cloud amount in the tropics from the CAM2.

[34] Significant errors in Cs are found in both the warm El Niño phase and cold La Niña phase. The changes of Cs from the cold phase to the warm phase in all three models are overly positive in the equatorial eastern Pacific. This deficiency may result from the deficiency in the low cloud scheme. We note that compared to the CAM2, the changes in Cs from the cold phase to the warm phase in two CAM3 models are improved in the central Pacific, and this improvement corresponds to an enhanced response of middle cloud cover in this region to El Niño warming. The response in the middle level clouds in the T42 CAM3 is about twice as large as in the CAM2, and the response in the T85 CAM3 is about 1.5 times as large as in the T42 CAM3. The middle level cloud cover response to El Niño warming in the T42 CAM3 is closer to the observed than the CAM2. The main difference between CAM3 and CAM2 exists in the parameterization of the convective cloud. Convective cloud fraction is proportional to the convective detrainment rate above 500 hPa following *Rasch and Kristjansson* [1998] in the CAM2 while it is related to updraft mass flux in the deep and shallow cumulus schemes according to a functional form suggested by *Xu and Krueger* [1991] in the CAM3 [*Collins et al.*, 2004]. *Xu and Krueger* [1991] have shown that the cumulus mass flux is a good indicator for the convective cloud amount because it is a direct measure of the convection intensity. Using a numerical cumulus ensemble model, they also have demonstrated that other large-scale variables, including the relative humidity, large-scale vertical velocity and surface precipitation are not good indicators for convective cloud amount. Therefore the improvement of middle cloud cover in the CAM3 is likely a consequence of the revision of convective clouds parameterization from the CAM2 to the CAM3. It is also interesting to note that a change in the resolution considerably increases the response of the middle level cloud cover to El Niño warming.

[35] El Niño warming causes a major disruption of the tropical hydrological cycle and this disruption is relatively well observed. Models may have to simulate adequately the response of the tropical hydrological cycle to this warming in order to be reliable tools for predicting the response of the hydrological cycle to global warming. By contrasting three successive NCAR models, it is encouraging to see that

Figure 21. (a) Response of high cloud amount to El Niño warming from ISCCP observations, (b) CAM2, (c) T42 CAM3, and (d) T85 CAM3. Shown are regression coefficients obtained by linearly regressing high cloud amount at each grid point against the underlying SST averaged over the region of El Niño warming (160°–290°E, 5°S–5°N). The interannual variations of high cloud amount over the ERBE period are used for the calculations. The observations are the same as those used by *Sun et al.* [2003].

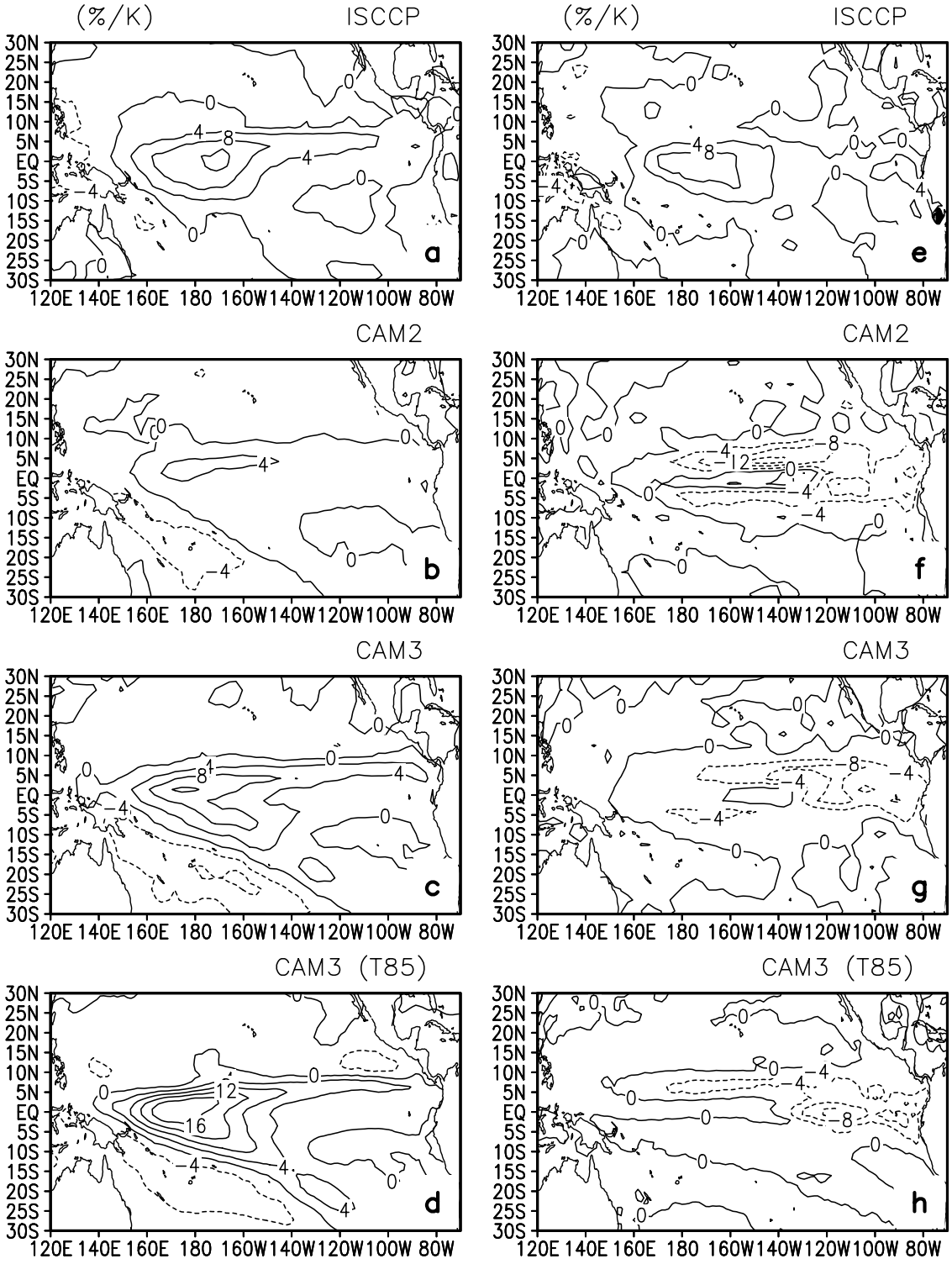

Figure 22. Response of (a–d) the middle and (e–h) the low cloud amount to El Niño warming from ISCCP observations, CAM2, T42 CAM3, and T85 CAM3. Shown are regression coefficients obtained by linearly regressing the middle and low cloud amount at each grid point against the underlying SST averaged over the region of El Niño warming (160°–290°E, 5°S–5°N). The interannual variations of middle and low cloud amount over the ERBE period are used for the calculations. The observations are the same as those used by *Sun et al.* [2003].

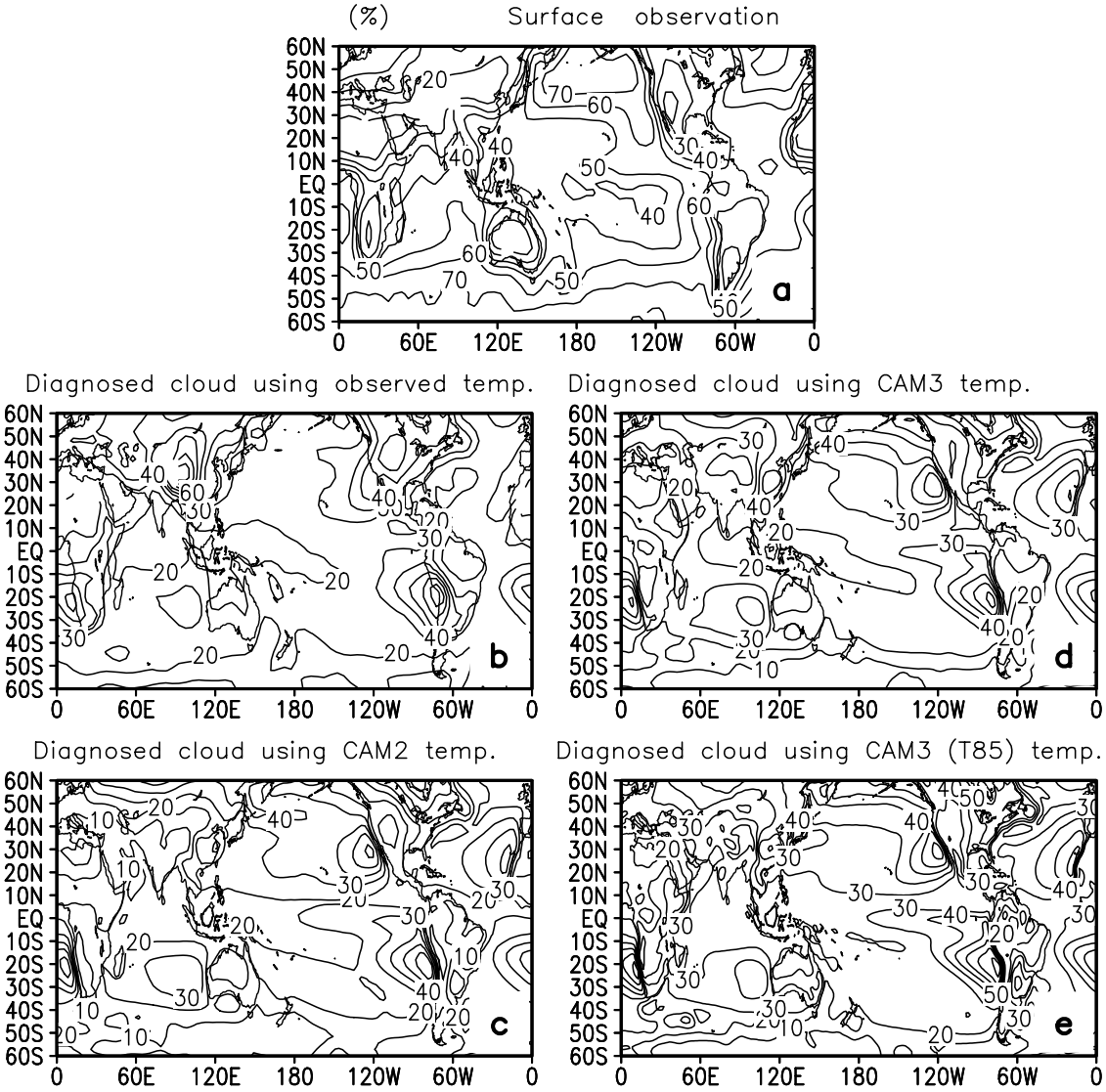

Figure 23. (a) Spatial pattern of annual mean (1971–1996 mean) low-level cloud amount from surface observations [*Dai and Trenberth*, 2004]. Also shown are the low-level marine stratocumulus cloud amount diagnosed using *Klein and Hartmann*'s [1993] scheme (b) with the observed surface and the NCEP-NACR reanalysis 700 mbar potential temperatures (1971–1996 mean) and with the corresponding simulated potential temperatures (1979–1996 mean) from (c) CAM2, (d) T42 CAM3, and (e) T85 CAM3 (see text for more details).

significant progresses have been made, though significant problems remain. Precipitation efficiency (the ratio between changes in the upper tropospheric humidity and changes in the precipitation) and the vertical distribution of clouds (the ratio between changes in the upper and lower level clouds) appear to be the key problems in the models that need to be further improved.

[36] The present analysis concerns the changes in water vapor and cloud radiative forcing over the ERBE period in response to ENSO forcing. We will extend the analysis to other period with newly available data from CERES (Clouds and the Earth's Radiant Energy System) [*Wielicki et al.*, 1996]. We also plan to use the Tropical Rainfall Measuring Mission (TRMM) data [*Kummerow et al.*, 2000] to examine the vertical distribution of diabatic heating [*Tao et al.*, 2001; *Shige et al.*, 2004]. The annual cycle poses another test of the models' ability in simulating the variability in the tropical hydrological cycle, and it will be examined in a further study. Also, the current study has focused on the analysis over the tropical Pacific. Our next step is to extend the analysis on the whole tropics and the entire globe. The global broadband surface emissivity from NASA Langley Research Center and global surface temperature from Climatic Research Unit (CRU) are available for us. The annual cycle of surface temperature can also be used as the forcing signal [*Inamdar and Ramanathan*, 1998]. Therefore it is possible to extend the present analysis to the entire globe. This will help to gain a more comprehensive evaluation of the models' capability in simulating the response of water vapor and clouds to El Niño warming,

contributing to a better assessment of the model predictions of the response of the tropical hydrological cycle to global warming.

[37] **Acknowledgments.** This research was supported partially by NOAA's office of global programs (the Climate Dynamics Program and Experimental Prediction Program, and the CLIVAR Pacific Program), and partially by the NSF Climate Dynamics Program (ATM-9912434 and ATM-0331760). The authors would like to thank William Collins and James Hack for providing the T85 CAM3 simulations, John Fasullo for providing the ISCCP data and Aiguo Dai for providing the surface observations data during the course of this study.

References

Barkstrom, B. R. (1984), The Earth Radiation Budget Experiment (ERBE), *Bull. Am. Meteorol. Soc.*, *65*, 1170–1185.

Boville, B. A., and P. R. Gent (1998), The NCAR Climate System Model, version one, *J. Clim.*, *11*, 1115–1130.

Boville, B. A., P. J. Rasch, J. J. Hack, and J. R. McCaa (2006), Representation of clouds and precipitation processes in the Community Atmosphere Model (CAM3), *J. Clim.*, *19*, 2184–2198.

Briegleb, B. P. (1992), Delta-Eddington approximation for solar radiation in the NCAR Community Climate Model, *J. Geophys. Res.*, *97*, 7603–7612.

Cess, R. D., et al. (1990), Intercomparison and interpretation of climate feedback processes in 19 atmospheric general-circulation models, *J. Geophys. Res.*, *95*, 16,601–16,615.

Cess, R. D., et al. (1996), Cloud feedback in atmospheric general circulation models: An update, *J. Geophys. Res.*, *101*, 12,791–12,794.

Charlock, T. P., and V. Ramanathan (1985), The albedo field and cloud radiative forcing produced by a general circulation model with internally generated cloud optics, *J. Atmos. Sci.*, *42*, 1408–1429.

Chou, M. D. (1994), Coolness in the tropical Pacific during an El Niño episode, *J. Clim.*, *7*, 1684–1692.

Clough, S. A., F. X. Kneizys, and R. W. Davies (1989), Line shape and the water vapor continuum, *Atmos. Res.*, *23*, 229–241.

Collins, W. D. (2001), Parameterization of generalized cloud overlap for radiative calculations in general circulation models, *J. Atmos. Sci.*, *58*, 3224–3242.

Collins, W. D., and A. K. Inamdar (1995), Validation of clear-sky fluxes for tropical oceans from the Earth Radiation Budget Experiment, *J. Clim.*, *8*, 569–578.

Collins, W. D., J. K. Hackney, and D. P. Edwards (2002), An updated parameterization for infrared emission and absorption by water vapor in the National Center for Atmospheric Research Community Atmosphere Model, *J. Geophys. Res.*, *107*(D22), 4664, doi:10.1029/2001JD001365.

Collins, W. D., et al. (2003), Description of the NCAR Community Atmosphere Model (CAM2), report, 189 pp., Natl. Cent. for Atmos. Res., Boulder, Colo. (Available at http://www.ccsm.ucar.edu/models/atm-cam/docs/cam2.0/description.pdf)

Collins, W. D., et al. (2004), Description of the NCAR Community Atmosphere Model (CAM 3.0), *Tech. Rep. NCAR/TN-464+STR*, 210 pp., Natl. Cent. for Atmos. Res., Boulder, Colo.

Collins, W. D., P. J. Rasch, B. A. Boville, J. J. Hack, J. R. McCaa, D. L. Williamson, B. P. Briegleb, C. M. Bitz, S.-J. Lin, and M. H. Zhang (2006a), The formulation and atmospheric simulation of the Community Atmosphere Model version 3 (CAM3), *J. Clim.*, *19*, 2144–2161.

Collins, W. D., et al. (2006b), The Community Climate System Model version 3 (CCSM3), *J. Clim.*, *19*, 2122–2143.

Dai, A., and K. E. Trenberth (2004), The diurnal cycle and its depiction in the Community Climate System Model, *J. Clim.*, *17*, 930–951.

Gates, W. L. (1992), AMIP: The Atmospheric Model Intercomparison Project, *Bull. Am. Meteorol. Soc.*, *73*, 791–794.

Hack, J. J. (1994), Parameterization of moist convection in the National Center for Atmospheric Research Community Climate Model (CCM2), *J. Geophys. Res.*, *99*, 5551–5568.

Hack, J. J., J. T. Kiehl, and J. W. Hurrell (1998), The hydrologic and thermodynamic characteristics of the NCAR CCM3, *J. Clim.*, *11*, 1179–1206.

Hack, J. J., J. M. Caron, S. G. Yeager, K. W. Oleson, M. M. Holland, J. E. Truesdale, and P. J. Rasch (2006a), Simulation of the global hydrological cycle in the CCSM Community Atmosphere Model version 3 (CAM3): Mean features, *J. Clim.*, *19*, 2199–2221.

Hack, J. J., J. M. Caron, G. Danabasoglu, K. W. Oleson, C. M. Bitz, and J. E. Truesdale (2006b), CCSM-CAM3 climate simulation sensitivity to changes in horizontal resolution, *J. Clim.*, *19*, 2267–2289.

Hartmann, D. L., M. E. Ockert-Bell, and M. L. Michelsen (1992), The effect of cloud type on Earth's energy balance: Global analysis, *J. Clim.*, *5*, 1281–1304.

Inamdar, A. K., and V. Ramanathan (1998), Tropical and global scale interactions among water vapor, atmospheric greenhouse effect, and surface temperature, *J. Geophys. Res.*, *103*, 32,177–32,194.

Ji, M., A. Leetmaa, and J. Derber (1995), An ocean analysis system for seasonal to interannual climate studies, *Mon. Weather Rev.*, *123*, 460–481.

Kalnay, E., et al. (1996), The NCEP/NCAR 40-year reanalysis project, *Bull. Am. Meteorol. Soc.*, *77*, 437–471.

Kiehl, J. T. (1994), On the observed near cancellation between longwave and shortwave cloud forcing in tropical regions, *J. Clim.*, *7*, 559–565.

Kiehl, J. T., and P. R. Gent (2004), The Community Climate System Model, version two, *J. Clim.*, *17*, 3666–3683.

Kiehl, J. T., and K. E. Trenberth (1997), Earth's annual global mean energy budget, *Bull. Am. Meteorol. Soc.*, *78*, 197–208.

Kiehl, J. T., J. J. Hack, G. Bonan, B. A. Boville, D. Williamson, and P. J. Rasch (1998a), The National Center for Atmospheric Research Community Climate Model: CCM3, *J. Clim.*, *11*, 1131–1149.

Kiehl, J. T., J. J. Hack, and J. W. Hurrell (1998b), The energy budget of the NCAR Community Climate Model: CCM3, *J. Clim.*, *11*, 1151–1178.

Klein, S. A., and D. L. Hartmann (1993), The seasonal cycle of low stratiform clouds, *J. Clim.*, *6*, 1587–1606.

Kummerow, C., et al. (2000), The status of the Tropical Rainfall Measuring Mission (TRMM) after two years in orbit, *J. Appl. Meteorol.*, *39*, 1965–1982.

Ramanathan, V., and W. Collins (1991), Thermodynamic regulation of ocean warming by cirrus clouds deduced from observations of the 1987 El Niño, *Nature*, *351*, 27–32.

Ramanathan, V., R. D. Cess, E. F. Harrison, P. Minnis, B. R. Barkstrom, E. Ahmad, and D. Hartmann (1989), Cloud-radiative forcing and climate: Results from the Earth Radiation Budget Experiment, *Science*, *243*, 57–63.

Ramaswamy, V., and S. M. Freidenreich (1991), Solar radiative line-by-line determination of water vapor absorption and water cloud extinction in inhomogeneous atmosphere, *J. Geophys. Res.*, *96*, 9133–9157.

Rasch, P. J., and J. E. Kristjansson (1998), A comparison of the CCM3 model climate using diagnosed and predicted condensate parameterizations, *J. Clim.*, *11*, 1587–1614.

Raval, A., and V. Ramanathan (1989), Observational determination of the greenhouse effect, *Nature*, *342*, 758–762.

Rossow, W. B., and R. A. Schiffer (1999), Advances in understanding clouds from ISCCP, *Bull. Am. Meteorol. Soc.*, *80*, 2261–2288.

Rossow, W. B., A. W. Walker, D. E. Beuschel, and M. D. Roiter (1996), International Satellite Cloud Climatology Project (ISCCP) documentation of new cloud datasets, *Rep. WMO/TD-737*, 115 pp., World Meteorol. Organ., Geneva, Switzerland.

Shige, S., Y. N. Takayabu, W.-K. Tao, and D. E. Johnson (2004), Spectral retrieval of latent heating profiles from TRMM PR data. Part I: Development of a model-based algorithm, *J. Appl. Meteorol.*, *43*, 1095–1113.

Slingo, J. M. (1987), The development and verification of a cloud prediction scheme for the ECMWF model, *Q. J. R. Meteorol. Soc.*, *113*, 899–927.

Soden, B. J. (1997), Variations in the tropical greenhouse effect during El Niño, *J. Clim.*, *10*, 1050–1055.

Stocker, T. F., et al. (2001), Physical Climate processes and feedbacks, in *Climate Change 2001: The Scientific Basis*, edited by J. T. Houghton et al., pp. 417–470, Cambridge Univ. Press, New York.

Sun, D.-Z., and K. E. Trenberth (1998), Coordinated heat removal from the equatorial Pacific during the 1986–87 El Niño, *Geophys. Res. Lett.*, *25*, 2659–2662.

Sun, D.-Z., C. Covey, and R. S. Lindzen (2001), Vertical correlations of water vapor in GCMs, *Geophys. Res. Lett.*, *28*, 259–262.

Sun, D.-Z., J. Fasullo, T. Zhang, and A. Roubicek (2003), On the radiative and dynamical feedbacks over the equatorial cold-tongue, *J. Clim.*, *16*, 2425–2432.

Sun, D.-Z., T. Zhang, C. Covey, S. A. Klein, W. D. Collins, J. J. Hack, J. T. Kiehl, G. A. Meehl, I. M. Held, and M. Suarez (2006), Radiative and dynamical feedbacks over the equatorial cold-tongue: Results from nine atmospheric GCMs, *J. Clim.*, in press.

Tao, W.-K., S. Lang, W. S. Olson, R. Meneghini, S. Yang, J. Simpson, C. Kummerow, E. Smith, and J. Halverson (2001), Retrieved vertical profiles of latent heat release using TRMM rainfall products for February 1998, *J. Appl. Meteorol.*, *40*, 957–982.

Trenberth, K. E., J. Fasullo, and L. Smith (2005), Trends and variability in column-integrated atmospheric water vapor, *Clim. Dyn.*, *24*, 741–758.

Uppala, S. M., et al. (2005), The ERA-40 reanalysis, *Q. J. R. Meteorol. Soc.*, *131*, 2961–3012, doi:10.1256/qj.04.176/.

Wentz, F. J. (1997), A well-calibrated ocean algorithm for special sensor microwave/imager, *J. Geophys. Res.*, *102*, 8703–8718.

Wielicki, B. A., B. R. Barkstrom, E. F. Harrison, R. B. Lee III, G. L. Smith, and J. E. Cooper (1996), Clouds and the Earth's Radiant Energy System (CERES): An Earth Observing System Experiment, *Bull. Am. Meteorol. Soc.*, *77*, 853–868.

Xie, P., and P. A. Arkin (1997), Global precipitation: A 17-year monthly analysis based on gauge observations, satellite estimates, and numerical model outputs, *Bull. Am. Meteorol. Soc.*, *78*, 2539–2558.

Xie, S., M. Zhang, J. S. Boyle, R. T. Cederwall, G. L. Potter, and W. Lin (2004), Impact of a revised convective triggering mechanism on Community Atmosphere Model, version 2, simulations: Results from short-range weather forecasts, *J. Geophys. Res.*, *109*, D14102, doi:10.1029/2004JD004692.

Xu, K.-M., and S. K. Krueger (1991), Evaluation of cloudiness parameterizations using a cumulus ensemble model, *Mon. Weather Rev.*, *119*, 342–367.

Zhang, G. J., and N. A. McFarlane (1995), Sensitivity of climate simulations to the parameterization of cumulus convection in the Canadian Climate Centre general circulation model, *Atmos. Ocean.*, *33*, 407–446.

D.-Z. Sun and T. Zhang, Physical Sciences Division, ESRL, NOAA-CIRES, Mail Code R/PSD1, 325 Broadway, Boulder, CO 80305, USA. (tao.zhang@noaa.gov)